AD NUMBER

AD916687

NEW LIMITATION CHANGE

TO

Approved for public release, distribution unlimited

FROM

Distribution authorized to U.S. Gov't. agencies only; test and evaluation; Dec 1973. Other requests shall be referred to RADC [DCCL], GAFB, NY 13441.

AUTHORITY

USAF, ltr, 12 Apr 1978.

RADC-TR-73-287
Final In-House Report
December 1973

WIDEBAND COHERENT COMMUNICATION AT VLF WITH THE EXPERIMENTAL TRANSMITTING ANTENNA MODULATOR (ETAM)

John T. Gamble

Laboratory Directors' Fund
Project 01710108

Rome Air Development Center
Air Force Systems Command
Griffiss Air Force Base, New York

WIDEBAND COHERENT COMMUNICATION AT VLF WITH THE EXPERIMENTAL TRANSMITTING ANTENNA MODULATOR (ETAM)

John T. Gamble

FOREWORD

This report effectively complements RADC-TR-72-212 entitled "Experimental Transmitting Antenna Modulator" which describes the design and in-plant testing of the antenna modulator as performed by Westinghouse Electric Corporation under contract F30602-72-C-0051. The effort described in this report is the in-house on-air performance evaluation of the contractor produced equipment. Thus, these in-house results add to the contractor efforts described in RADC-TR-72-212, to provide a complete coverage of the VLF/LF Transmitting Antenna broadbanding project sponsored under Laboratory Directors' Funding, 01710108.

The author is indebted to Mr. G. A. Pfeiffer, Captain W. A. Acree, and Sgt. R. Klumpp of RADC for their indispensable assistance in making the on-air measurements.

APPROVED:

GEORGE E. BRUNETTE
Chief, Communications Transmission Branch
Communications and Navigation Division

APPROVED:

FRED I. DIAMOND, Technical Director
Communications and Navigation Division

FOR THE COMMANDER:

CARLO P. CROCETTI
Chief, Plans Office

ABSTRACT

A 1-kilowatt Experimental Transmitting Antenna Modulator (ETAM) was tested on-air at RADC. This on-air performance evaluation at 29.5 kHz employed a VLF transmitting station at Camden, New York and a receiving station at RADC, Griffiss AFB, New York. Using the ETAM, an 800 baud coherent FSK (Modulation Index of 1/2) signal was efficiently transmitted over the 160 Hz 3 db static bandwidth transmitter/antenna system; concurrently, the signal was received and coherently demodulated with negligible evidence of intersymbol distortion or other system degradation. On the other hand, when the ETAM was removed from the transmission system, it was necessary to derate the tranamitter output power by 10 db to preclude destruction of the transmitter output transformer caused by the high-Q mismatched output load; under this operating condition, it was impossible to obtain bit error rates less than 6% because of the ambient atmospheric noise and intersymbol distortion. This report describes the equipment configurations at the transmitter and receiver, the test procedures, and the quantitative results.

TABLE OF CONTENTS

LIST OF ILLUSTRATIONS

LIST OF TABLES

SECTION I
INTRODUCTION

The objective of this effort was to evaluate the on-air performance of an Experimental Transmitting Antenna Modulator (ETAM) developed by Westinghouse Electric Corporation. This antenna modulator rapidly tunes a narrowband VLF/LF antenna system in synchronism with the transmitted FSK signals. The antenna modulation is performed with minimum insertion loss and is suitable for operation at any frequency in the 20-60 kHz range. It is designed to accommodate FSK signalling rates up to 1500 bits/sec and input powers up to one kilowatt.

A. The Report

Although the antenna modulator was successfully tested in-plant in conjunction with a high-Q simulated antenna load (a single-tuned series resonant circuit), this was not sufficient to assure its technical adequacy when interoperated with a real antenna system. Thus, this report describes the on-air testing of the antenna modulator. Specifically, it includes: (1) A description of the transmitting and receiving equipment; (2) A description of the instrumentation; (3) A qualitative assessment of the effect of the ETAM on the communication link, including photographs of the antenna current envelopes to illustrate system response; and (4) quantitative results consisting of the measured bit error rate performance of a coherent FSK modem with and without the ETAM in the system.

B. Significance of the Effort

This on-air test provides a real-world operational verification of the theoretical and laboratory feasibility of efficiently transmitting wideband FSK signals over an antenna system whose static bandwidth is much less than the signal bandwidth. The net effect of this technique is to greatly increase the effective bandwidth-efficiency product of VLF/LF transmitting antennas for FSK signalling; this effect, not realizable by linear, time-invariant circuit techniques, is achieved by utilizing time-variant antenna tuning inductance.

C. Background

Mathematical analysis has shown (see Appendix B) that modulation of high-Q tuned circuit reactance, if done to coincide with the appropriate carrier phase, can shift the instantaneous resonance of the circuit at any rate which is an integral subharmonic of twice the resonant frequency; in other words, such a reactance shift can be made after any arbitrary number of half-cycles of the resonant frequency. For a total shift, Δf, of the resonant frequency, f, if the driving voltage is of constant amplitude and shifted in frequency synchronously with the circuit tuning, then the envelope of the circuit current waveform has a transient whose maximum amplitude is given by $\Delta f/f$ relative to the steady state amplitude. In a practical FSK transmitting system where the total frequency shift is a small fraction of the nominal carrier (center) frequency, the resultant antenna current is nearly constant; in turn, the radiated signal (proportional to the antenna current) will have a similar approximately constant amplitude which is entirely suitable for coherent FSK demodulation.

Earlier practical efforts at implementing this technique, however, have been applied only to FSK at a signalling rate about the same as the antenna system 3 dB static bandwidth. This is shown in Table I where the characteristics of some operational high-powered VLF/LF stations are listed; these stations currently use antenna modulation for 50 baud (bits/sec) FSK signalling.

TABLE I
HIGH POWERED VLF/LF STATIONS (Reference 6)

Operator	Location	Power	3 dB Static Bandwidth
US Air Force	Hawes, California	100 KW	65 Hz @ 27 kHz
US Air Force	Silver Creek, Nebraska	100 KW	65 Hz @ 27 kHz
US Navy	Cutler, Maine	2 MW	70 Hz @ 18 kHz
US Navy	Annapolis, Maryland	200 KW	33 Hz @ 20 kHz

Thus, although theory predicts the feasibility of signalling rates much greater than antenna static bandwidths, current operational practice has employed antenna modulation for FSK signalling rates comparable to antenna static bandwidths; in these cases, the antenna modulation serves to minimize the instantaneous load phase angle at the transmitter amplifier outputs and hence, to maximize amplifier efficiencies.

On the other hand, the ETAM was specifically developed to investigate and implement the antenna modulation technique for wideband FSK signalling with statically narrowband VLF/LF antenna systems. (A complete description of the design and principle of operation is contained in RADC TR-72-212 (Reference 3), but for completeness in this report, a brief description is presented in Section II). The ETAM was tested in-plant, utilizing a single-tuned series resonant circuit to simulate a high-Q (100 Hz static bandwidth at 37 kHz) low frequency antenna circuit. This simulated antenna system was driven by a 1 KW solid state amplifier which in turn was excited by an FSK modulator; the ETAM was used to resonate the antenna circuit in synchronism with the FSK modulation. The system was operated at modulation reversal (alternating upward and downward frequency shifts) rates of 200, 1000, and 1600 bauds; the corresponding frequency shifts were 100, 500, and 800 Hz, respectively, and the input power was 1000 watts for the lower rates and 300 watts for the highest rate. The principal apparent distortion in the output (antenna current) was, as theoretically predicted, amplitude steps of less than 5% at the instants of frequency shift. The apparent insertion loss was less than .3 dB. Finally, a measurement of intersymbol distortion, D, was made according to

$$D = 1 - \frac{\int_0^T S_T(f,t)\, S_R(f,t)\, dt}{\int_0^T [S_R(f,t)]^2\, dt}$$

where:

$$S_I(f,t) = \begin{cases} A\cos 2\pi f_1 t & 0 \leq t \leq T \\ A\cos 2\pi f_2 t & t < 0 \end{cases}$$

$=$ Undistorted input signal to the antenna system

$S_R(f,t) = B\cos(2\pi f_1 t + \theta)$

$=$ Steady state antenna output Signal produced by the constant input signal $A\cos(2\pi f_1 t)$.

$S_T(f,t) =$ Output signal produced by the input signal $S_I(f,t)$ where

$$|f_2 - f_1| = \frac{1}{2T} \qquad (1)$$

This measurement yielded D < .05 for FSK signalling at 1000 bauds. The clear implication of these in-plant test results was that the ETAM should permit high efficiency (nearly equivalent to constant amplitude, constant frequency signal radiation) FSK transmission up to 1600 bauds over any antenna system whose static bandwidth was at least 100 Hz. Nevertheless, these satisfactory in-plant test results did not guarantee similar successful on-air performance. The effort described herein was thus undertaken to measure the real-world, on-air performance of the ETAM with random FSK modulation.

D. Significance

This report presents the practical validation of the ETAM design principle.

The earlier theoretical analyses, based on the principle of resonant transfer of stored electrical energy in reactive networks and the application of Laplace transforms to the time-variant system response clearly implied the physical validity of the ETAM approach. The contractor development and in-plant test with the simulated antenna network reduced the theoretical approach suggested in the literature to practice, wherein the reactance modulation rate was far greater than the static bandwidth of the passive simulation network. This present effort, then, finally applied the reactance modulation technique to a practical antenna system; moreover, this practical implementation of the ETAM involved significant input power -- much more than had been utilized in small-signal (10 watts or less) reactance amplifier approaches such as proposed by Vallese (Reference 5).

SECTION II
EQUIPMENT AND SUB-SYSTEM DESCRIPTION

The on-air test of the ETAM was conducted at the RADC Camden, New York, test annex and at RADC, Griffiss AFB, New York. The ETAM was operated in conjunction with the experimental low frequency transmitting station at Camden, and the transmitted signals were received at RADC. The following sections describe (A) the operational principle and design of the ETAM; (B) the equipment configuration at the transmitting station; and (C) the equipment configuration at the receiving station.

A. The Experimental Transmitting Antenna Modulator (ETAM)

1. Principle of Operation

In Figure 1, a passive network is shown which closely approximates the electrical characteristics of an electrically short monopole (or top-loaded monopole) antenna. The term "electrically short" is appropriate when the operating frequency is much less than the natural dipole resonance frequency of the antenna system, or, in other words, the length of the antenna is much less than 1/4 the free-space wavelength of the signal to be transmitted. Under this condition, the antenna structure is effectively a series capacitance and resistance. Because of the electrical shortness of the antenna, both the capacitance, C_a, and the radiation resistance, R_r, are necessarily small. The loss resistance, R_L, produced by ohmic losses in the antenna and ground system is customarily minimized in design and construction so as to maximize efficiency; the antenna efficiency is given by

$$\eta = \frac{R_r}{R_r + R_L} \tag{2}$$

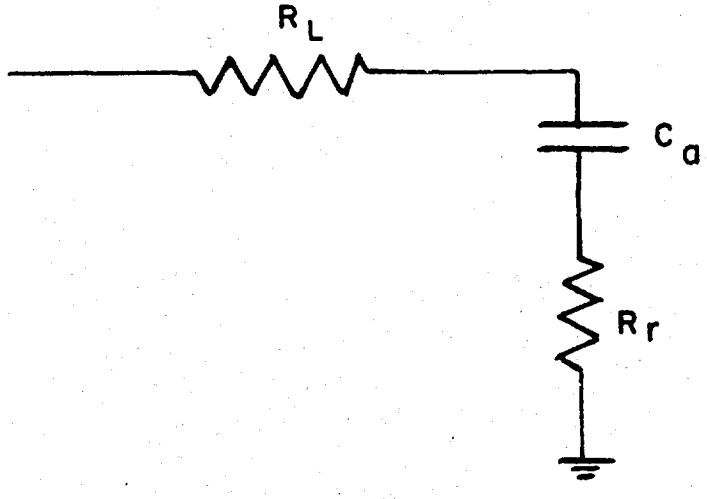

Figure 1. Passive Equivalent of Electrically Short Monopole

However, the low value of capacitance of the antenna structure causes such a short monopole to be a highly reactive electrical load for a power transmitter. This is compensated for by the inclusion of a series inductor or helix of proper inductance to produce series resonance, and hence a resistive transmitter load, at the desired frequency. This typical low frequency equivalent antenna circuit is shown in Figure 2.

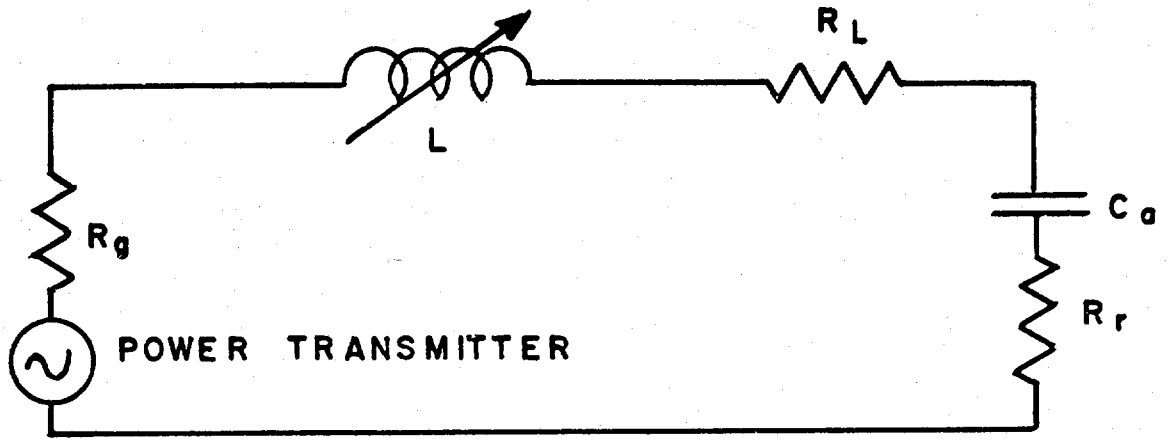

Figure 2. Passive Equivalent Circuit of a VLF/LF Antenna System

Just as the inherent antenna and ground losses must be minimized for system efficiency, so must the ohmic losses in the tuning inductance; in Figure 2, the resistance of the coil is combined with the other antenna system loss resistances in the term R_L. Here, the series resonant circuit is a very high-Q network where Q is defined by

$$Q \triangleq \frac{2\pi fL}{R_r + R_L + R_g} = \frac{1}{2\pi f C_a (R_r + R_L + R_g)} \qquad (3)$$

where R_g is the source resistance of the transmitter amplifier represented in its Thevenin equivalent form, and F is the operating frequency.

The static half-power (3 dB) bandwidth of this network is given by

$$B_3 \approx \frac{R_r + R_L + R_G}{2\pi L} = \frac{f}{Q} \qquad (4)$$

where $f = \frac{1}{2\pi\sqrt{LC_a}}$ is the operating frequency.

Customarily, such a fixed-tuned antenna system used for FSK transmission would be tuned to a frequency intermediate between the upper and lower FSK shift frequencies. This balances the degradation of the output signal amplitudes at the two shift frequencies, but it also results in the antenna system being slightly detuned from resonance at all times during FSK transmission. This prompted the development of antenna modulation to alleviate this situation. (As discussed in Section I, operational applications of this technique permit maximum FSK signalling rates comparable to the antenna static bandwidths).The following discussion describes the antenna modulation technique.

Consider the functional representation of Figure 3. The input to the system is a binary voltage waveform (digital data) which drives a frequency shift keying (FSK) modulator. The modulator produces two outputs: (1) a constant envelope radio-frequency sinusoid whose frequency is shifted in accordance with the input digital data and (2) a rectangular baseband waveform whose voltage is stepped up and down in synchronism with the frequency shifts of the FSK signal output. The FSK signal is then amplified and applied directly to the antenna system. On the other hand, the baseband output drives the antenna modulator whose function is to vary the effective inductance.

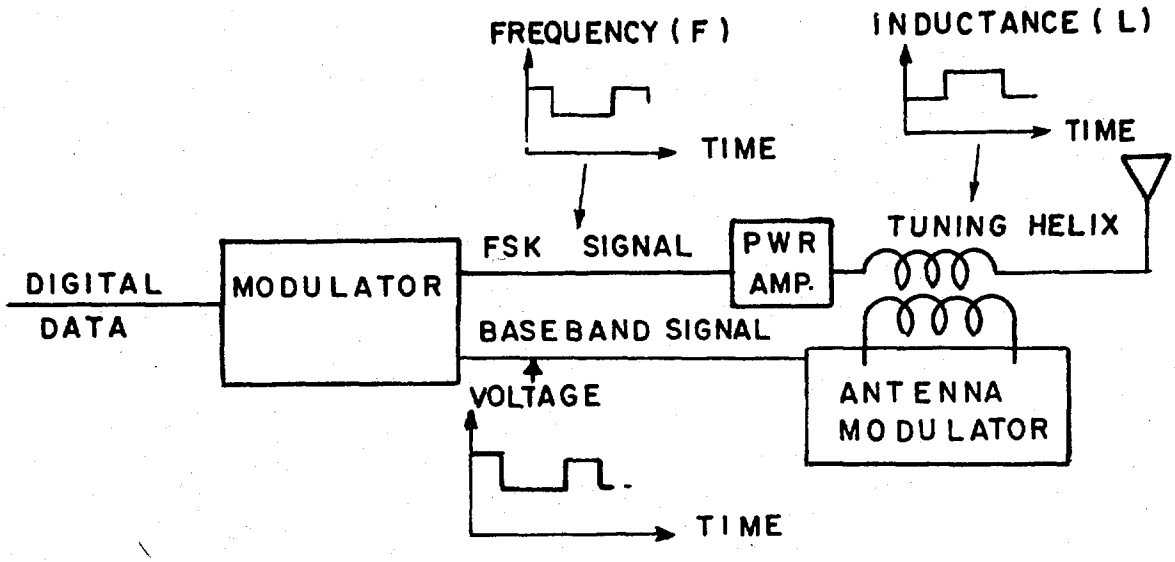

Figure 3. Antenna Modulator Design Principle

L, of the antenna system. This modulation of the circuit inductance is designed to cause the antenna system to be tuned to exact resonance at the FSK signal frequency. Thus, the output load of the power amplifier is resistive at all times.

The specific method of modulating inductance in the ETAM is to switch in and out a small amount of the total antenna series inductance (ΔL). This incremental inductance can be calculated directly by (Reference 3):

$$\Delta L \approx \frac{2\Delta f}{(2\pi)^2 f_1^{\,3} C_a} \tag{5}$$

where Δf is the difference between the upper and lower FSK frequencies and f_1 is the lower FSK frequency.

Physically, the inductance is changed by inductively coupled parasitic elements. Each element consists of a helix terminated by a solid state switch; when the switch is open, the parasitic coil does not affect the inductance of the main tuning helix but when the switch is closed, the parasitic element becomes an inductively coupled short circuit which reduces the effective inductance of the main helix. Thus, these parasitic elements permit the stepwise modulation of the overall tuning inductance by means of inductively-coupled, synchronously-controlled switches.

Figure 4 shows schematically the ETAM coupling method. Here we see the ETAM tuner coil of inductance L_1 connected in series with the main antenna tuning helix of inductance L_M. In the open switch condition, the total tuning inductance, L_T, is given by

$$L_T = L_1 + L_M \tag{6}$$

However, in the closed switch condition, the total inductance becomes

$$L = ML_1 + L_M, \; 0 \leq M \leq 1 \tag{7}$$

where M is the mutual inductive coupling between L_1 and the sub coil.

Hence, we have

$$\Delta L = L_T - L = (1 - M)L_1 \tag{8}$$

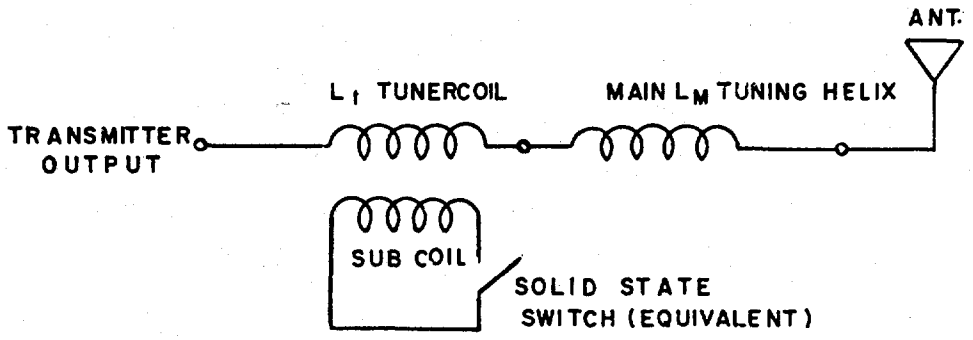

Figure 4. ETAM Coupling

Before proceeding to a more specific description of the ETAM equipment, it is appropriate to consider two important constraints in the operation of ETAM with a high-powered transmitting system. The first overall system constraint is that of signal waveform continuity. Because the antenna system is a high-Q load for the transmitter, it is mandatory that the RF waveform be continuous at all times, including frequency shift transitions. If this constraint is not observed, drastic antenna current amplitude and phase transients result which preclude efficient system operation and may be destructive to transmitter amplifiers operating at or near full power. The second constraint, specifically related to the ETAM operation, is that shifts of inductance must occur when the instantaneous current in the antenna circuit is nearly zero. The reason for this constraint is a corollary of the high-Q of the antenna circuit; because Q can also be defined as the ratio of the maximum energy stored in the reactive components, $1/2\ LI^2$ or $1/2CV^2$, to the average energy dissipated per radian of the signal waveform $RI^2/4\pi f$, where I is the current amplitude and f is the waveform frequency, substantial energy is stored in the magnetic field of the inductance on a time-periodic basis. This instantaneous stored energy in the magnetic field of the inductor is proportional to the square of the instantaneous antenna current; thus, the proper time for switching the inductance value is at a current zero. Conversely, a change of inductance, when the current is near its semi-periodic maximum magnitude, will result in voltage transients potentially destructive to switching components and excessive transients in the current envelope.

However, if inductance switches are constrained to occur at current zeros (this is an idealization, since any practical switch requires a finite time to change from "on" to "off" or *vice-versa),* then the expected maximum transient on the current envelope can be determined by stored energy considerations. If the current in the antenna circuit of Figure 2 is at steady state at the upper frequency, f_2, the total stored energy in the circuit is given by

$$U_2 = 1/2\ L\ I_2^{\,2} = 1/2\ C_a V_2^{\,2} \tag{9}$$

where $V_2 = I_2\ (R_T + R_L + R_G)$ and

$$f_2 = \frac{1}{2\pi\sqrt{LC_a}} \tag{10}$$

As previously stated, the total stored energy is in the magnetic field of the inductor when the current is maximum and the voltage zero; in the case where the current is zero and the voltage at the antenna base is maximum, the total stored energy is in the electrostatic field of the antenna structure-grounding system. Considering the case where the current is maximum (I_2), we have from (9) and (10):

$$I_2 = \sqrt{\frac{2U_2}{L}} = 2\pi f_2 \sqrt{2U_2 C_a} \tag{11}$$

Now, if the inductance is instantaneously increased from L to L + ΔL at the next current zero crossing, the circuit immediately becomes resonant at frequency F_1 given by

$$f_1 = \frac{1}{2\pi\sqrt{(L + \Delta L) C_a}} \tag{12}$$

However, the circuit energy cannot change appreciably during the next quarter RF cycle (because of high circuit Q) so that the peak current at the end of the quarter cycle is given by

$$I_2' = \sqrt{\frac{2U_2}{L + \Delta L}} = 2\pi f_1 \sqrt{2U_2 C_a} \tag{13}$$

Thus, the ratio of the current after a downward frequency shift to the current just before the shift is given by

$$\frac{I_2'}{I_2} = \frac{f_1}{f_2} = \frac{f_2 - (f_2 - f_1)}{f_2} = 1 - \frac{f_2 - f_1}{f_2} \tag{14}$$

Now, assuming $f_2 - f_1 \ll f_2$, then $f_1 \approx f_2 \approx \frac{1}{2}(f_1 + f_2) \triangleq f$ (15)

(where f is the nominal unmodulated carrier frequency), and

$$\frac{I_2'}{I_2} \approx 1 - \frac{f_2 - f_1}{f} \tag{16}$$

Now, considering the alternate situation where the current is at steady state at the lower frequency f_1, we obtain $U_1 = 1/2(L + \Delta L) I_1^2 = 1/2\, C_a V_1^2$ so that $I_1 =$

$$\sqrt{\frac{2U_1}{L + \Delta L}} = 2\pi f_1 \sqrt{2U_1 C_a} \tag{17}$$

Again postulating a change of inductance at a current zero, but this time a decrease by ΔL, we obtain the maximum current a quarter cycle later

$$I_1' = \sqrt{\frac{2U_1}{L}} = 2\pi f_2 \sqrt{2U_1 C_a} \tag{18}$$

Here, the ratio of the current after an *upward* frequency shift to the current just before the shift is given by

$$\frac{I_1'}{I_1} = \frac{f_1}{f_2} = \frac{f_2 + (f_1 - f_2)}{f_2} \approx 1 + \frac{f_2 - f_1}{f} \tag{19}$$

Since $f_2 - f_1 \ll f$, the latter term of both (16) and (19) will be a small fraction of the steady state current amplitude, but this is the maximum transient effect to be expected on the antenna current envelope. It should

be noted that this transient term in the current amplitude expression is only applicable at a frequency shift point: with increasing time, the transient component decays to zero in accordance with the circuit Q so that the overall current tends to its steady state amplitude. Thus, the effect of circuit Q is to limit the recovery rate of the current envelope to steady state after a frequency shift; however, it is obvious that the maximum current amplitude transient represents a very small fraction of the overall current amplitude. Hence, the output current envelope is nearly constant and for the analysis of phase coherent modem systems, a constant envelope approximation is valid.

2. Description of Equipment

A 1-kilowatt model of the ETAM tuner was built for both laboratory and field test evaluation. This equipment consisted of the following major assemblies:

a. Tuner Coil. This coil, shown in Figure 6, consists of a primary winding and an inductively coupled subcoil. The subcoil is connected to an RF switch which changes the antenna tuning as described in this section (Section II).

b. RF Switching Assembly. This switch connects to the above tuner subcoil for changing the primary winding inductance value, which provides the required antenna tuning in accordance with FSK requirements. The basic switching circuit, as included in Figure 4, consists of two thyristors and two diodes in a d-c forward biased configuration. In the "on" state, the switch is an open circuit. This switch remains in either state until implemented by either an "on" or an "off" pulse. The circuit elements used to provide an operating RF switch are shown connected to the RF coil in Figure 5.

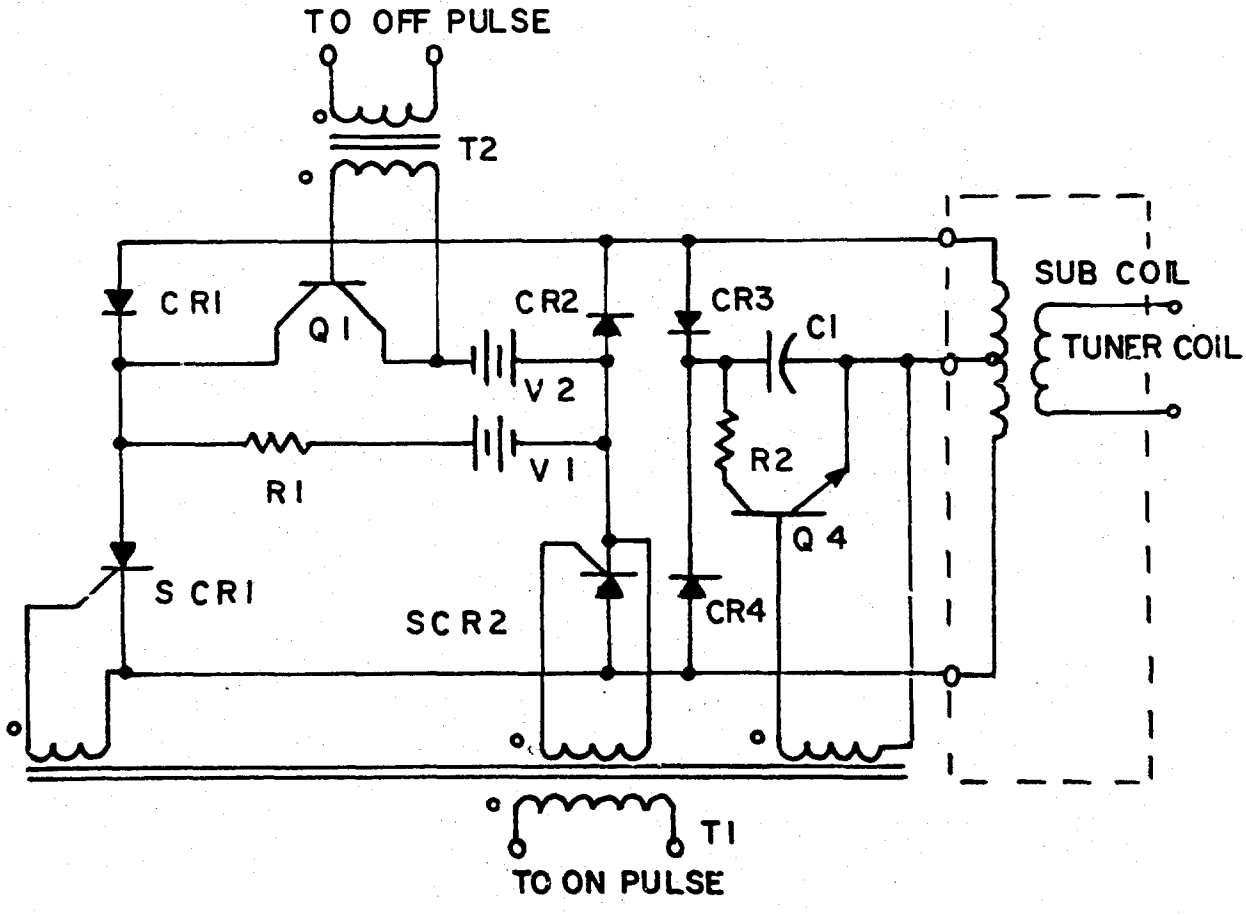

Figure 5. RF Switch Schematic

This circuit performs the following three basic functions:

(1) Turn-On. Turn-on is initiated by applying a single positive pulse to the gates of SCR1 and SCR2 simultaneously. This causes these SCR's to start conducting in the forward direction, resulting in a d-c latching current provided by the source V1 around the loop R1, SCR1 and SCR2. Steering diodes CR1 and CR2 are used to restrict this latching current to the SCR loop only. This latching current (approximately 3 amperes) is sufficient to maintain continuous conduction in the SCR's. The circuit now performs as a closed bi-directional switch to the RF current supplied by the subcoil, with one polarity of the RF cycle flowing through CR1 and SCR1, and the opposite polarity flowing through CR2 and SCR2. This switch will remain in this closed state until the latching current is interrupted sufficiently long to permit each half of the RF cycle to pass through zero.

(2) Turn-Off. To return the RF switch to the "off" state, a positive pulse is applied to the base of Q1, which conducts and hence removes the latching current to SCR1 and SCR2. The turn-off time is reduced by returning the base of Q1 to a negative voltage (V2) which provided some forced turn-off commutation for SCR1 and SCR2. The switch is now open and will remain in this state until an "on" pulse is applied.

(3) Dynamic Damping. This part of the circuit is used to suppress voltage overshoot when the switch transfers from the "on" state to the "off" state. Although a transition occurs when the switch current is zero, a step function in voltage occurs when the switch stops conducting. This is due to the 90° phase relationship between the voltage and the current. The step function, unless suppressed, will subject the SCR's to voltage transients in excess of their rating, which can result in device destruction. This transient is suppressed by charging C1, using a full-wave rectifier circuit consisting of CR3 and CR4, and occurs during the RF switch transition from the "on" to the "off" state. As the transistor Q4 is off during the entire RF switch "off" state, capacitor C1 will charge to the peak open circuit voltage of the subcoil. This charge is removed during the RF switch "on" state by applying a positive pulse to the base of Q2 of sufficient duration (approximately 100 usec) thus reducing this capacitor voltage to zero as required for transient suppression during the next RF switch transition from "on" state to the "off" state.

The RF switch assembly, as shown in Figure 6, is air cooled by a self-contained fan.

c. Control Cabinet. This cabinet, also shown in Figure 6, contains all of the controls, power supplies, logic, and pulse drivers as required to operate the RF switches.

d. Zero Crossing Detector. This unit consists of a current transformer, which samples the antenna current, and a full-wave detector connected to the secondary of this current transformer. The output, therefore, supplies zero pulses every 180° of the operating frequency and is used as one of the inputs to both the "on" and the "off" logic.

A summary of the pertinent ETAM characteristics is presented in Table II below:

TABLE II
ETAM EQUIPMENT RATING SUMMARY

AC power source	60 Hz 120 V 5 A
Antenna current	6A RMS min. – 26 A RMS max.
Tuning coil RF voltage to ground	500 V RMS max.
Tuning coil PRI inductance (switch open)	92 μH
Tuning coil PRI inductance (switch closed)	91.6 μH max. 37.5 μH min.
Data input impedance	100 ohms
Data input voltage	(Positive) min. 4 V max. 6 V

TABLE II
ETAM EQUIPMENT RATING SUMMARY (Continued)

Data input pulse width (usec)	2 min., 10 max.
RF switch current	20 A (peak) max.
RF switch voltage	600 V (peak) max.
RF frequency range	20 kHz to 60 kHz
Square wave input voltage (test)	4 min., 10 max.
Square wave input impedance (test)	2 kohms

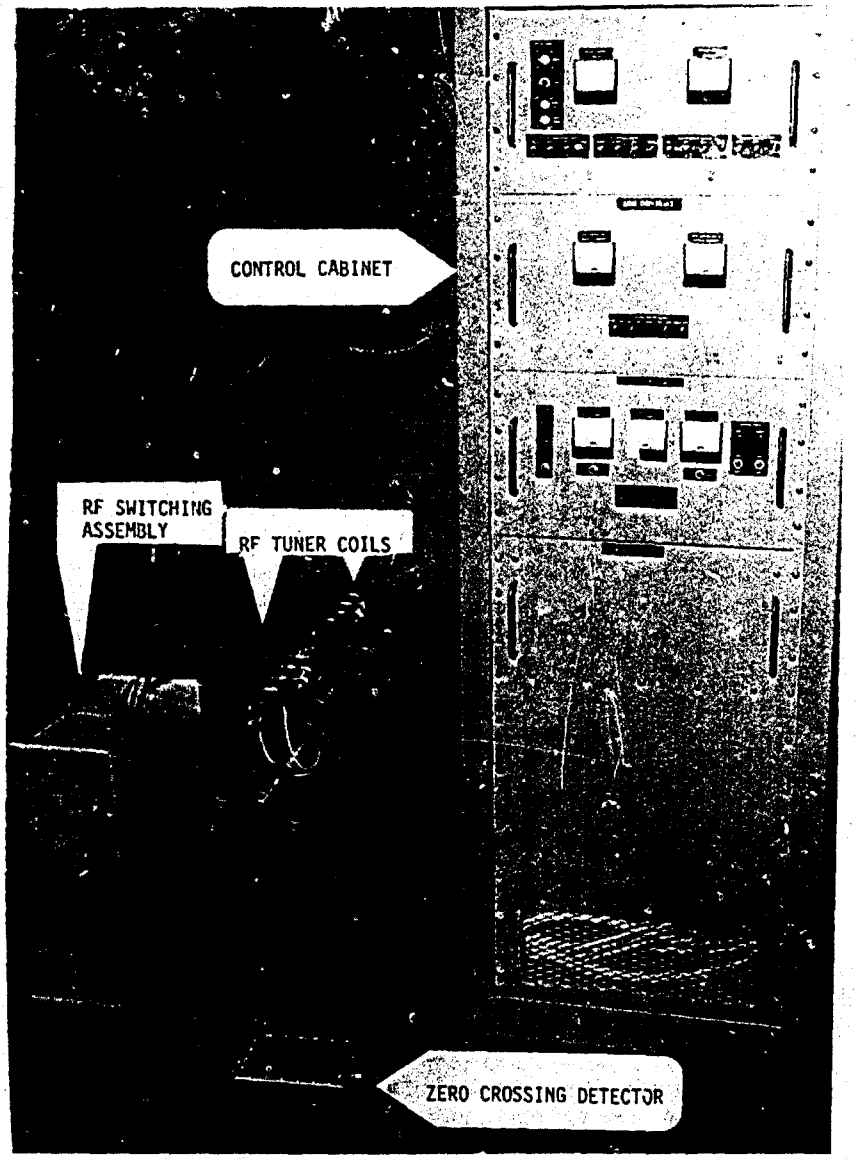

Figure 6. ETAM Equipment

B. The Transmitting Station

The ETAM was installed at the Camden, New York experimental VLF/LF transmitting station. Figure 7 is a block diagram of the overall transmitting system.

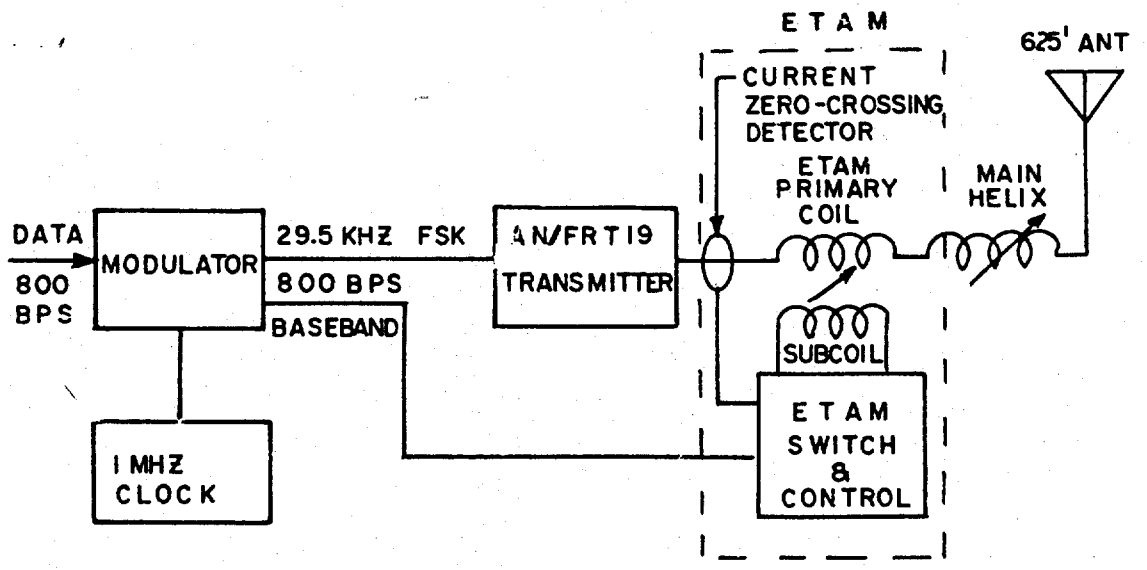

Figure 7. Transmitting System

The following is a brief description of the signals and equipment represented on the diagram (except for the ETAM components previously described):

1. Data. The data which was used to drive the modulator consisted of baud synchronous (all elements of equal length) digital data at a rate of 800 bauds (elements/second). The data was formatted into frames of 15 elements each where the fifteenth element was a binary 1 synchronization pulse.

2. Modulator. The special modulator generated two outputs, the FSK signal for RF transmission and a baseband rectangular voltage waveform synchronous with the FSK modulation (see Figure 3). The 800 baud FSK signal was derived by precise digital frequency division from a stable 1 MHz clock (or oscillator); this technique gives the spectral components of the FSK signal a coherent time base such that coherent demodulation by a suitable receiver is possible. The modulation index of the FSK waveform was .5 which means that the difference between the upper and lower FSK frequencies in Hz is equal to one half the baud rate. (In this system, the total difference between FSK frequencies was exactly 400 Hz.) Here, the upper shift frequency corresponds to a binary "0" and the lower shift frequency to a "1".

3. Clock. The 1 MHz Clock (or oscillator) was a Hewlett-Packard 5100A.

4. Transmitter. The AN/FRT-19 Low Frequency Transmitter is a linear Class B 15 KW tube-type amplifier. It is designed to operate in the nominal range of 30 kHz to 300 kHz.

5. Main Helix. The main tuning helix consisted of air-core Litz-wire coils for coarse tuning and a ferrite-loaded varicoupler for fine tuning. The mean inductance of this component of the system was 4100 μh.

6. Antenna. The low frequency antenna is a 625 foot top-loaded monopole with the following characteristics at 29.5 kHz:

- Static Capacitance – 7000 $\mu\mu$f
- Radiation Resistance – .114Ω
- 3 dB Static Bandwidth – 160 Hz
- Radiation System Efficiency (CW signal) – 5%
- Maximum Base Voltage – 30 KV

C. The Receiving Station

The FSK signal was received and demodulated by a receiver subsystem located at Griffiss AFB, New York, some 26 miles from the transmitting station at Camden. Figure 8 is a block diagram of the receiver subsystem.

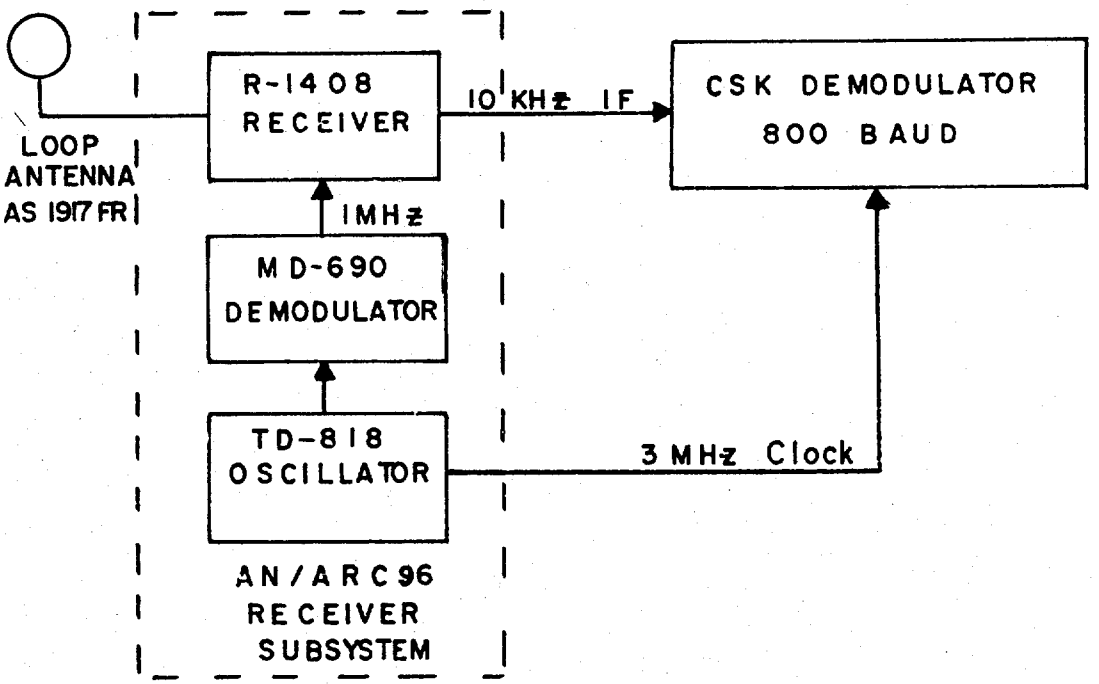

Figure 8. Receiving System

The various components of this receiving system are discussed below:

1. Loop Antenna. The receiving antenna was a crossed loop system, model AS1917FR, which is used operationally in the 487L Survivable Low Frequency Communication System ground receiving stations.

2. Receiver. The R-1408/ARC-96 Receiver is a VLF/LF receiver designed for operation in the 14-60 kHz range. It was operated in conjunction with the depicted MD-690/ARC-96 and TD-818/ARC-96 components which constitute an integral part of the AN/ARC-96 (airborne portion of the 487L system) receiver subsystem; however, for this test, the only function of the TD-818/ARC-96 and MD-690/ARC-96 was to provide the essential 1 MHz clock signal to the R-1408 receiver and the 3 MHz clock signal to the special 800 baud CSK demodulator as shown in Figure 8. The essential output of the R-1408 receiver was a hard-limited 10 kHz IF signal. Figure 9 shows a plot of the normalized frequency response of the R-1408 receiver, $H(f)\,H(f)^*/H(0)H(0)^*$ – where H(f) is the receiver complex transfer function, in a linear mode of operation (the hard limiter was inoperative for this measurement); from this data, the effective noise bandwidth of the receiver was calculated to be 469 Hz, substantially less than the FSK transmission rate.

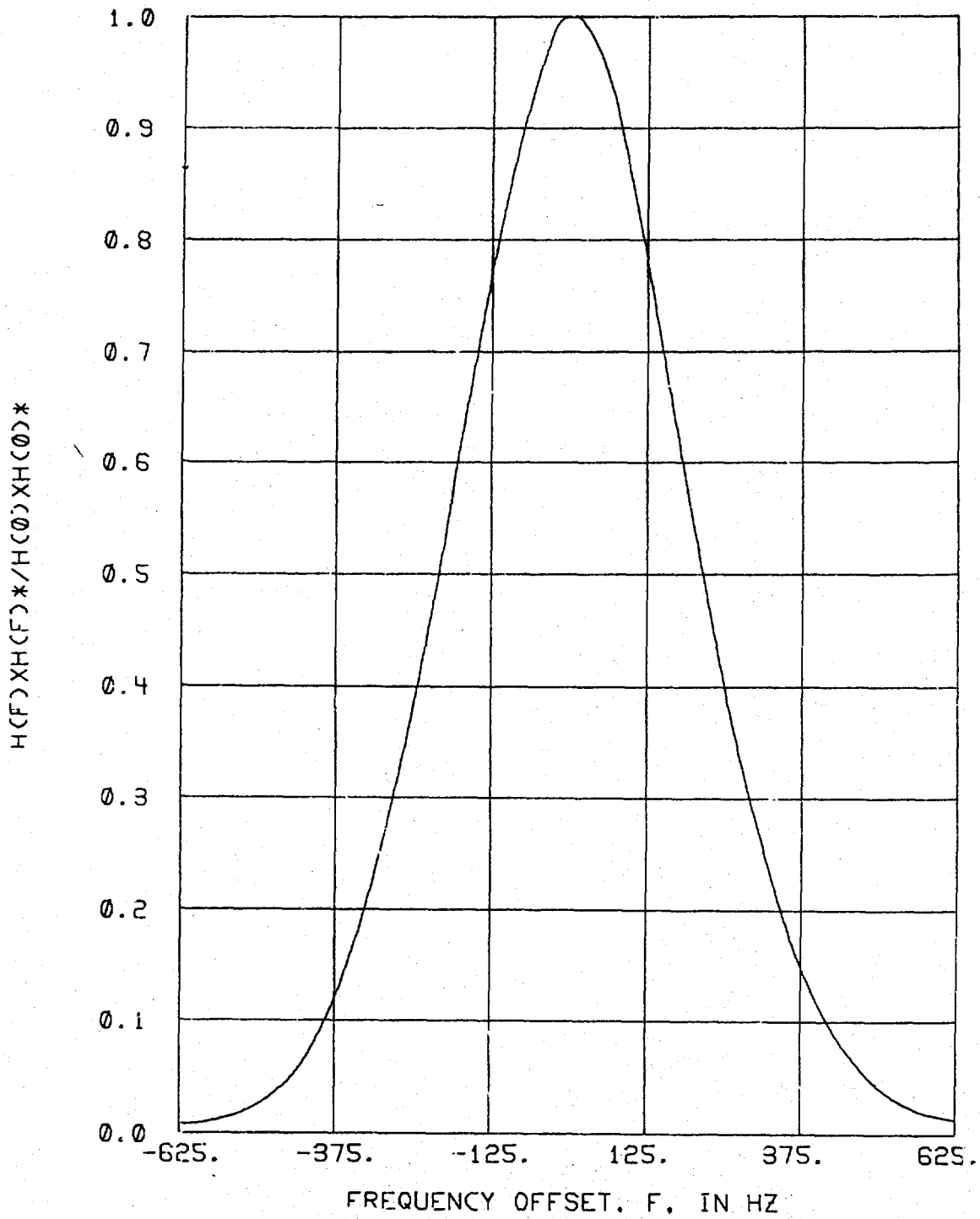

Figure 9. Receiver Frequency Response

3. CSK Demodulator. The 800 baud Compatible Shift Keying (CSK) demodulator coherently demodulated the 800 baud FSK signalling from the hard-limited 10 kHz IF signal. The CSK demodulation process is described in Appendix A, and its detection efficiency in Gaussian noise is shown to be virtually equivalent to the theoretically-optimum coherent biphase or quadriphase shift keying (PSK) detection.

SECTION III
TEST OPERATION AND INSTRUMENTATION

The instrumentation employed in this evaluation was intended to derive quantitative performance data on the modem system in a back-to-back configuration and on a real-world Low Frequency radio link wherein the ETAM was employed.

A. Back-to-Back Configuration

The back-to-back testing was intended to determine the modem and receiver performance under ideal conditions in a Gaussian noise environment. This phase of the evaluation provided a baseline for determining the effect of the ETAM on system performance. Figure 10 is a block diagram of the back-to-back test set-up.

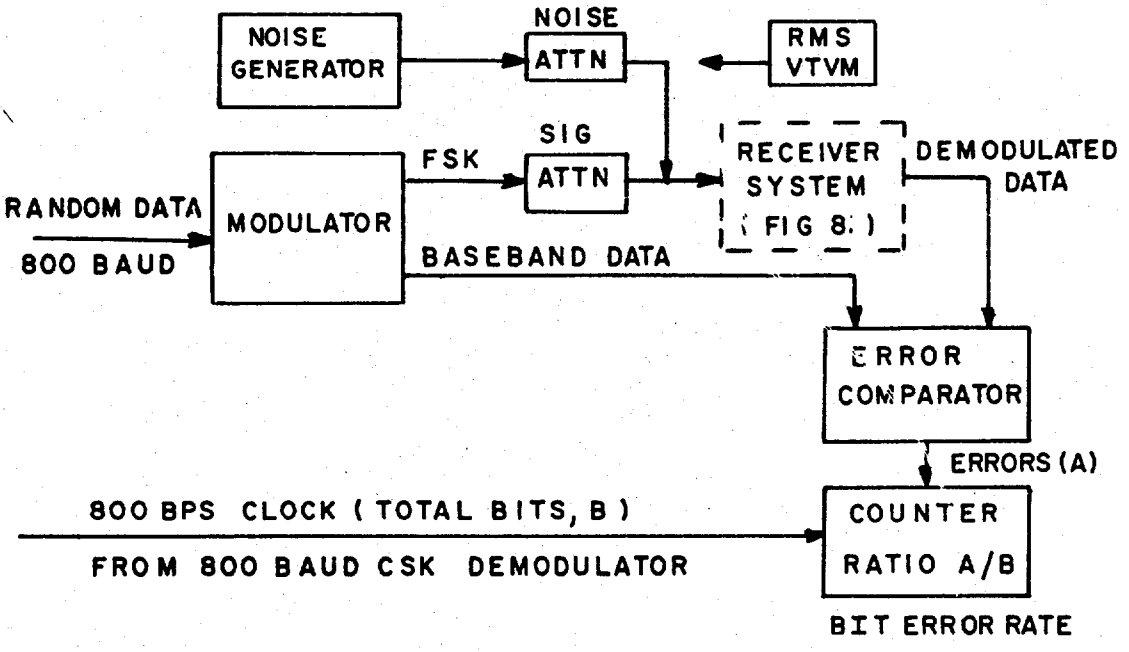

Figure 10. Back-to-Back Configuration

Here, the input to the modulator of Figure 7 is a random binary sequence at 800 baud. The FSK output of the modulator is then attenuated and added to White Gaussian noise at the input to the receiver system of Figure 8. The demodulated data out of the receiver system then becomes one of the two inputs to the bit error comparator. The other input to the bit error comparator is the baseband data output of the modulator. Within the error comparator, the baseband data is delayed in time to compensate for the processing delay in the Receiver system and then this delayed baseband data is compared with the demodulated data to yield a direct indication of bit errors. This error count was then divided by the total error count in a Hewlett-Packard 5233L Electronic Counter to yield a bit error rate. By varying the relative attenuation of the signal and noise channels, a bit error rate vs signal-to-noise ratio characteristic for the modem system was derived.

B. On-Air Test Configuration

The on-air test configuration was similar to the back-to-back set-up, except for the following: (1) the modulator and signal attenuator were replaced by the total transmitting system of Figure 7 plus the receiving

antenna of Figure 8, and (2) the baseband data link of Figure 10 included a wideband microwave link to carry the binary reference data to the error comparator co-located with the receiver system. Figure 11 is a block diagram of the on-air test configuration.

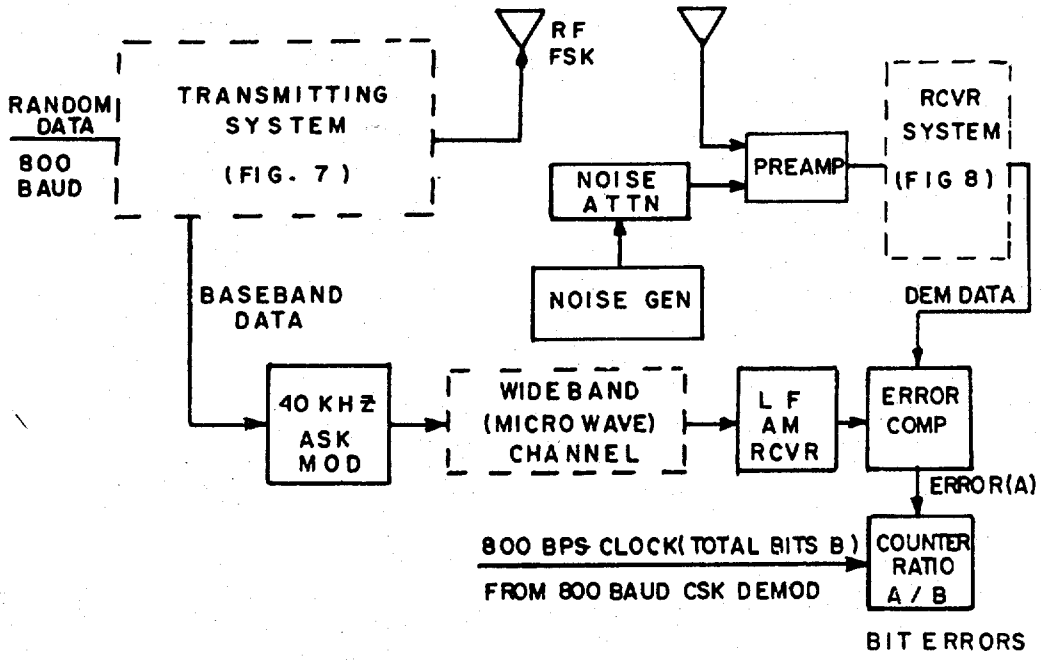

Figure 11. On-Air Configuration

In this latter configuration, the baseband data was used to produce an on-off-keyed (or Amplitude Shift Keyed, ASK) waveform at a carrier frequency of 40 kHz. This signal was then transmitted via a wideband (50 kHz bandwidth channel) microwave link from the Camden, New York, test facility to Griffiss AFB and the microwave-baseband output was detected at 40 kHz by a Honeywell 6869 VLF Receiver; because of the 40-50 dB signal-to-noise ratio at the Honeywell receiver output, this demodulated signal provided a virtually error-free binary reference for comparison with the signal processed through the Low Frequency Transmitter/Receiver system (Figures 7 and 8). Again, the counter yielded the bit error rate – but in this case, it was the bit error rate, on-air, and with the ETAM in operation.

SECTION IV
QUALITATIVE RESULTS

Although this evaluation was primarily intended to determine the quantitative effect of the ETAM on VLF/LF system performance, some qualitative observations of the ETAM performance are of significant interest. These include the observed antenna current transient response with and without the ETAM operating, the received signal envelope with and without the ETAM operating, and the effects of installation on ETAM operation and reliability.

A. Antenna Current Transient Response

As developed in Section II, the expected maximum current transient relative to steady state current, ΔI, is given by

$$\Delta I = \frac{f(t_o^+) - f(t_o^-)}{f} I \qquad (20)$$

where $f(t_o^+)$ is the frequency immediately following a frequency shift at time t_o from the frequency $f(t_o^-)$ just prior to t_o and I is the steady state current amplitude.

In the system under test, f = 29.5 kHz, and $|f(t_o^+) - f(t_o^-)| = 400$ Hz so that, the maximum relative transient would be

$$\left|\frac{\Delta I}{I}\right| = \frac{400}{29500} = .0136 \qquad (21)$$

Figures 12 and 13 are oscilloscope photographs of the actual antenna current envelope with the ETAM in operation. Figure 12 shows an "idle" baseband data sequence and the corresponding antenna current envelope where fourteen bits are spaces (upper FSK frequency) and each fifteenth bit is a mark (lower FSK frequency). Figure 13 shows the antenna current envelope for a random FSK sequence more typical of actual communication signals. In both cases, it can be seen that the actual transient in the antenna current is very minimal. Although the current envelope photographs do not give sufficient resolution to accurately measure the transient effect and verify the theoretical prediction of a 1.36% step, they do qualitatively show that the maximum antenna current amplitude transient will be very small.

On the other hand, the current response of a 160 Hz bandwidth network to an 800 baud FSK input signal would reasonably be expected to be substantially distorted in comparison with the response of a resistive, or infinite bandwidth network. Similarly, the VLF antenna system with a static bandwidth of 160 Hz and without the aid of the ETAM, should also have a substantially distorted current response to the 800 baud signal. This is clearly shown by the current envelope photographs of Figures 14 and 15. Figure 14 shows an "idle" data sequence and the corresponding antenna current envelope. Figure 15 shows a random baseband data sequence and corresponding antenna current envelope. The amplitude distortion on the current output produced by the narrow static bandwidth is clearly apparent.

Thus, the efficacy of the ETAM in maintaining a nearly constant maximal current in an otherwise band-limiting antenna system is graphically shown.

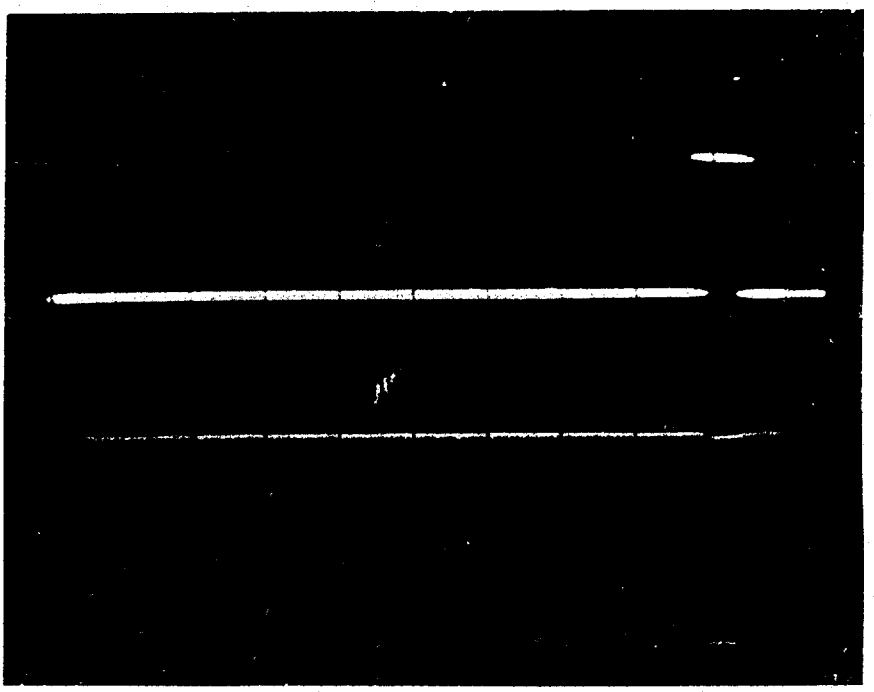

Figure 12. Antenna Current Envelope without ETAM – "Idle" Data

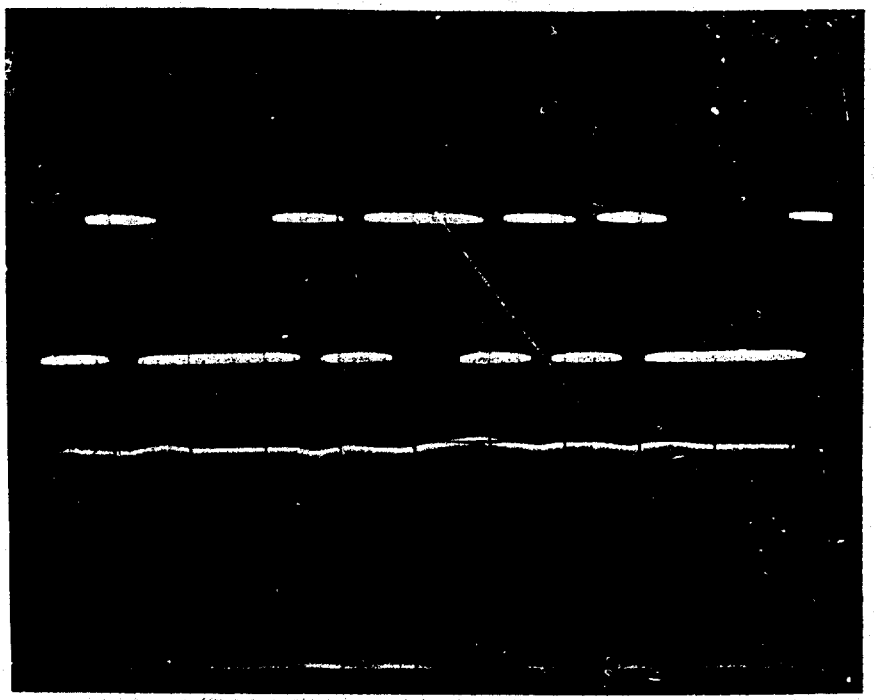

Figure 13. Antenna Current Envelope with ETAM – Random Data

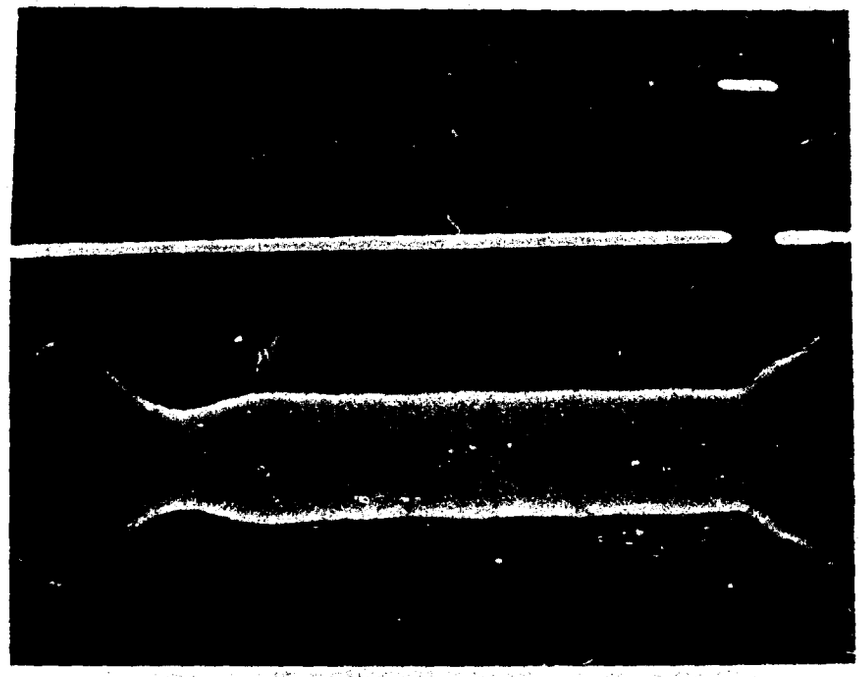

Figure 14. Antenna Current Envelope without ETAM – "Idle" Data

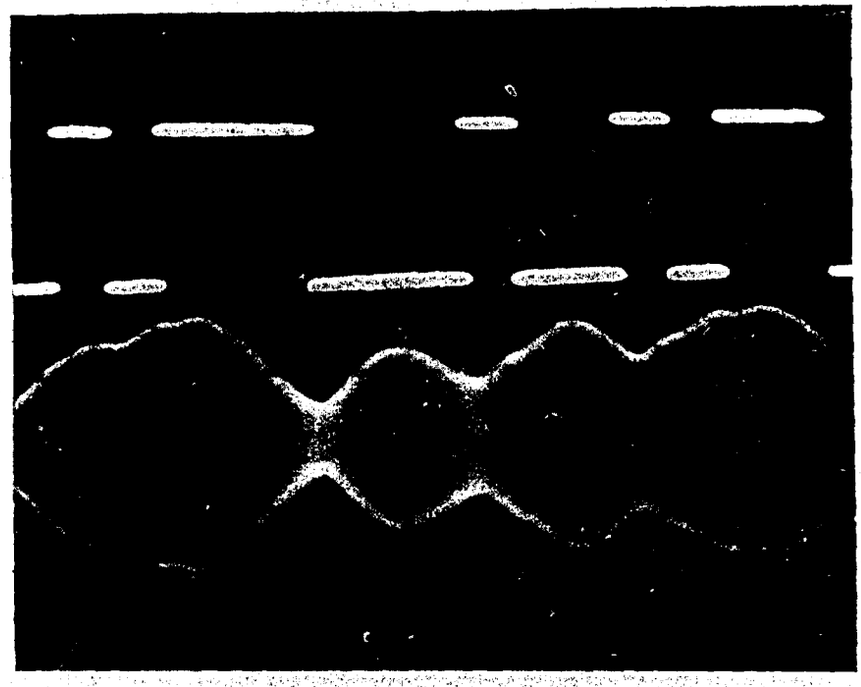

Figure 15. Antenna Current Envelope without ETAM – Random Data

B. Received Signal

In addition to antenna current envelopes, observations were made of the envelope of the signal as received in the antenna "far-field" at Griffiss AFB, N.Y. Because of the low radiation efficiency of the Camden transmitter system at 29.5 kHz, the maximum radiated power with the ETAM (observing the maximum antenna current limitation of 25 amperes from Table II) was only 71 watts. This resulted in a signal-to-atmospheric noise ratio on the order of 15-20 dB at the Griffiss based receiver, and thus perturbations of the observed signal envelope were as much due to received noise as to transient effects produced by the ETAM. Moreover, received signal transients which clearly corresponded to FSK frequency shifts are believed to be primarily the response of the Honeywell 6869 receiver to FSK modulation rather than an indication of transmitted signal envelope distortion. Nevertheless, the oscilloscope photographs do indicate the relative significance of frequency shifts in producing envelope transients on the received signal.

Figure 16 is an integrated (multiple exposure to compensate for low signal/noise ratio) photograph of the envelope of the 29.5 kHz signal in a 3 kHz receiver bandwidth (Honeywell 6869) where the FSK modulation corresponded to the "idle" data pattern (i.e. 14 upper frequency space bits and one lower frequency mark bit); the upper trace shows the corresponding demodulated signal. It can be seen that the maximum perturbation of the received current envelope (located approximately 4 msec earlier (left) on the lower trace which corresponds to the differential demodulation delay) is minimal for the frequency downshift and upshift 1.25 msec later. This clearly affirms the previous contention that the radiated signal, just as the transmitting antenna current, is nearly constant when the ETAM is employed in the system.

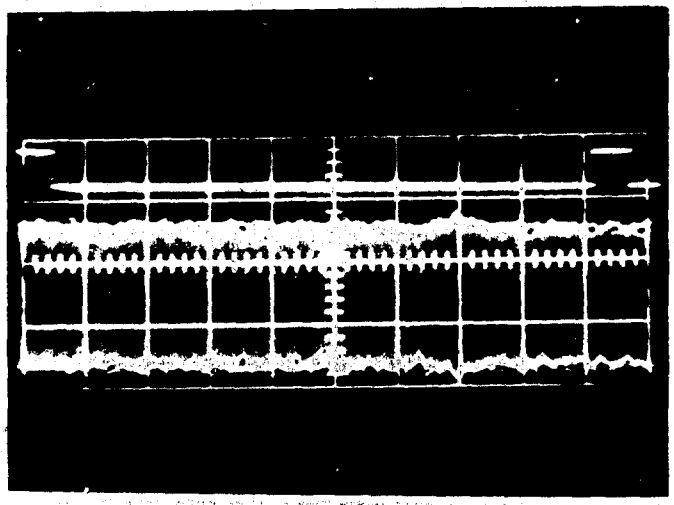

Figure 16. Received Signal Envelope with ETAM – "Idle" Data

On the other hand, operation of the system without the ETAM produced the integrated oscilloscope photograph of Figure 17 for the "idle" pattern. The similarity of this received signal envelope to the antenna current envelope of Figure 14 is readily apparent. In both instances, the unmodulated narrow band antenna system produced a significant amount of pulse-stretching which is apparent in the case of the isolated "mark" binary data element. (It should be noted that the rectangularity of the demodulated data elements (upper trace of the oscilloscope presentation) in Figures 16-17 is a result of pulse reshaping in the CSK demodulator).

Based on the observed characteristics of the received signal, it is apparent that the ETAM does permit the transmission of high rate FSK at VLF/LF over high-Q antenna systems with a minimum of amplitude distortion. Although this implies that the overall transmitter system with the ETAM may be nearly as effective as a true wideband (antenna static bandwidth substantially greater than the FSK signalling rate) antenna system of the

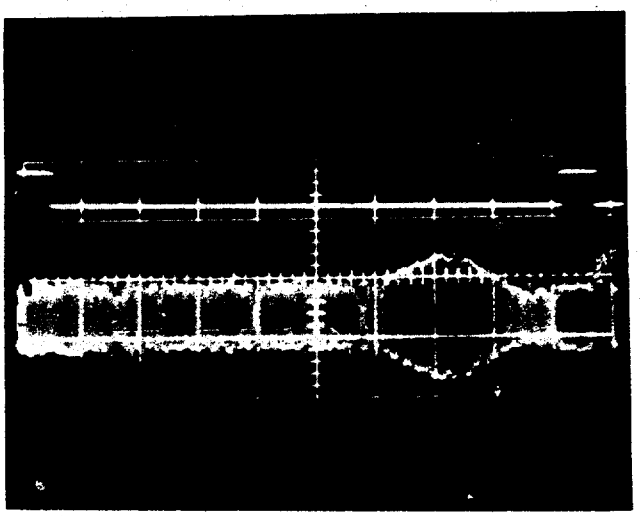

Figure 17. Received Signal Envelope without ETAM – "Idle" Pattern

same "on-tune" radiation efficiency, these qualitative amplitude results cannot really verify the quantitative modem system performance, especially in conjunction with the hard-limiting operational R1408 receiver. (However, the quantitative bit error rate results presented in Section V do show this implication to be true).

C. Effects of Installation on ETAM Operation and Reliability

In addition to the preceding observations which were pertinent to validating the functional principles of the ETAM, there were other factors bearing on the design and installation of both the 1KW model ETAM and any higher powered version. These included: (1) problems of false switching caused by RFI from the adjacent high powered transmitter; (2) difficulty in adjusting the two parallel parasitic coils for equilization of current division during conduction (switches on); and (3) difficulty in rapid identification of the inoperative switch in case of a silicon controlled rectifier (SCR) failure. Since these problems could be effectively handled in a future design, it is appropriate here to provide a brief discussion and a most likely design correction.

1. False Switching Produced by RFI. During the course of the on-air evaluation (three weeks) some4 SCR's failed, although these devices were operated well below their maximum current-voltage ratings. Because false triggering of the switches caused by RFI pickup in the ETAM control circuitry was noted at times, it is believed that this was the principal cause of SCR failure. The reason for this suspicion is that closing the SCR switches at a high instantaneous current point on an antenna current cycle would require the nearly instantaneous dissipation of substantial energy stored in the magnetic field of the tuning inductance. Mathematically, this energy would be specified by

$$U = 1/2\ \Delta L I^2 \qquad (22)$$

where I is the instantaneous antenna circuit current and ΔL is the change of inductance produced by the ETAM.

In order to preclude RFI-induced false triggering, it is essential that all small-signal control circuitry be completely RFI shielded to isolate it from an adjacent high power transmitter. Likewise, such shielding might be necessary in a higher-powered system to prevent positive feedback from the high power sections of the antenna modulator itself.

2. Current Division in Parallel Parasitic Elements. A difficulty noted in the adjustment of the ETAM was in achieving approximately equal inductive coupling of the two parasitic coils to the main tuning helix. An imbalance in coupling will produce a corresponding imbalance in current division between the parallel elements; obviously, this could cause component current-voltage ratings to be exceeded in individual switch sections even though the composite (parallel coil and switch) system rating is not exceeded. Although current imbalance is not believed to have been the primary cause of SCR failures in the on-air test, it may well have been a contributory factor. However, proper current division is believed to be the most significant technical risk area in a high-powered antenna modulator system wherein multiple parallel switches must be used. For this reason, gang tuning and integrated feedback control are believed to be essential in a high-powered implementation of the ETAM technology.

3. Identification of Inoperative Switches. In the ETAM on-air tests, the failure of a solid state switch necessitated a lengthy "trouble-shooting" procedure to identify the inoperative section. Since the ETAM employs only two such switching sections, this already lengthy diagnostic procedure would be a small fraction of that required for a high-powered system of tens to hundreds of similar switch sections. Thus, it was apparent that suitable functional indicators would have been very useful for ETAM operation and maintenance; it is also clear that functional indicators and protective circuitry, to prevent current overloads resulting from component failures, is mandatory in a high-powered antenna modulator system.

SECTION V
QUANTITATIVE RESULTS

The preceding in-plant tests of the ETAM and the qualitative performance results of Section IV all inspired confidence that the ETAM could greatly enhance the efficient transmission and reception of wideband FSK signals. However, with the exception of the in-plant "intersymbol distortion test" described in Section I, all of the in-plant and qualitative results thus far only verified that wideband FSK could be transmitted and not necessarily received and demodulated at high efficiency. This determination of detection efficiency was the principal question left unanswered by the in-plant tests on a simulated antenna system, and was, of course, the principal motivation behind the presently described on-air evaluation. Moreover, this evaluation employed coherently detectable FSK signals derived from random binary data, rather than the deterministic, but non coherent, modulation reversal signals of the in-plant test; thus, the on-air tests were fully representative of state-of-the-art VLF/LF communication technology because of the use of realistic signalling sequences, coherent modems, and the advanced R-1408 operational receiver. The specific results presented here consist of measured bit error rates as a function of signal-to-noise ratio where the noise is additive white Gaussian noise. By employing the instrumentation and operational procedures described in Section III, bit error rates were measured for the 800-bit coherent FSK system both back-to-back and on-air.

Figure 18 is a plot of bit error rates versus signal-to-noise ratio referenced to the detection bandwidth, or 800 Hz. The measured performance, both back-to-back and on-air with the ETAM, is seen to be approximately .8 dB less efficient than theoretically ideal (Ref. Appendix A). However, it is clearly apparent that operation with a narrow band radiation system and the ETAM affords modem efficiency just as high as obtained with a true wideband channel (typified by the back-to-back test configuration). Moreover, this modem efficiency is achieved without a significant reduction in transmitting antenna system radiation efficiency; that is, the wideband FSK signal can be radiated at nearly the same power as a narrow band CW signal for the same power input to the antenna system. Hence, this quantitative result, when integrated with the low insertion loss and high antenna system output efficiency for FSK implied by the qualitative results of Chapter IV (and by the in-plant tests on the simulated antenna, Ref. 3), indicates that the ETAM does afford a significant enhancement of system efficiency for wideband FSK signalling. In comparison with resistive loading of the antenna system (and consequent power dissipative loss) to achieve a minimal 800 Hz antenna static bandwidth (necessary for 800 baud FSK), the ETAM afforded an increase of efficiency by a factor of 5, or 7 dB.

To further illustrate the impact of the ETAM on system performance, the transmitting system was operated with the 800 baud FSK signal, but without the ETAM. Here, the adverse effects were twofold. First, in order to avoid destructive over-heating of the transmitter amplifier output transformer and varicoupler, it was necessary to derate the transmitter output by 10 dB; this was a direct result of the continuous impedance mismatch of the high-Q antenna system for the wideband FSK output of the transmitter. Secondly, the minimum achievable bit error rate in the coherent receiver system was greater than 6% – unacceptably high for teletype communication; this error rate was apparently a result of the intersymbol distortion produced by the narrow band transmitting antenna system.

In conclusion, the on-air test demonstrated qualitatively and quantitatively the practical feasibility of high-rate tuning inductance modulation of high-Q VLF/LF transmitting antenna systems for synchronous wideband FSK signalling. Under this condition, optimum transmitting system radiation efficiency was maintained and optimum signal modulation and demodulation was achieved. The quantitative system improvement provided by the ETAM in this on-air test was at least 7 dB.

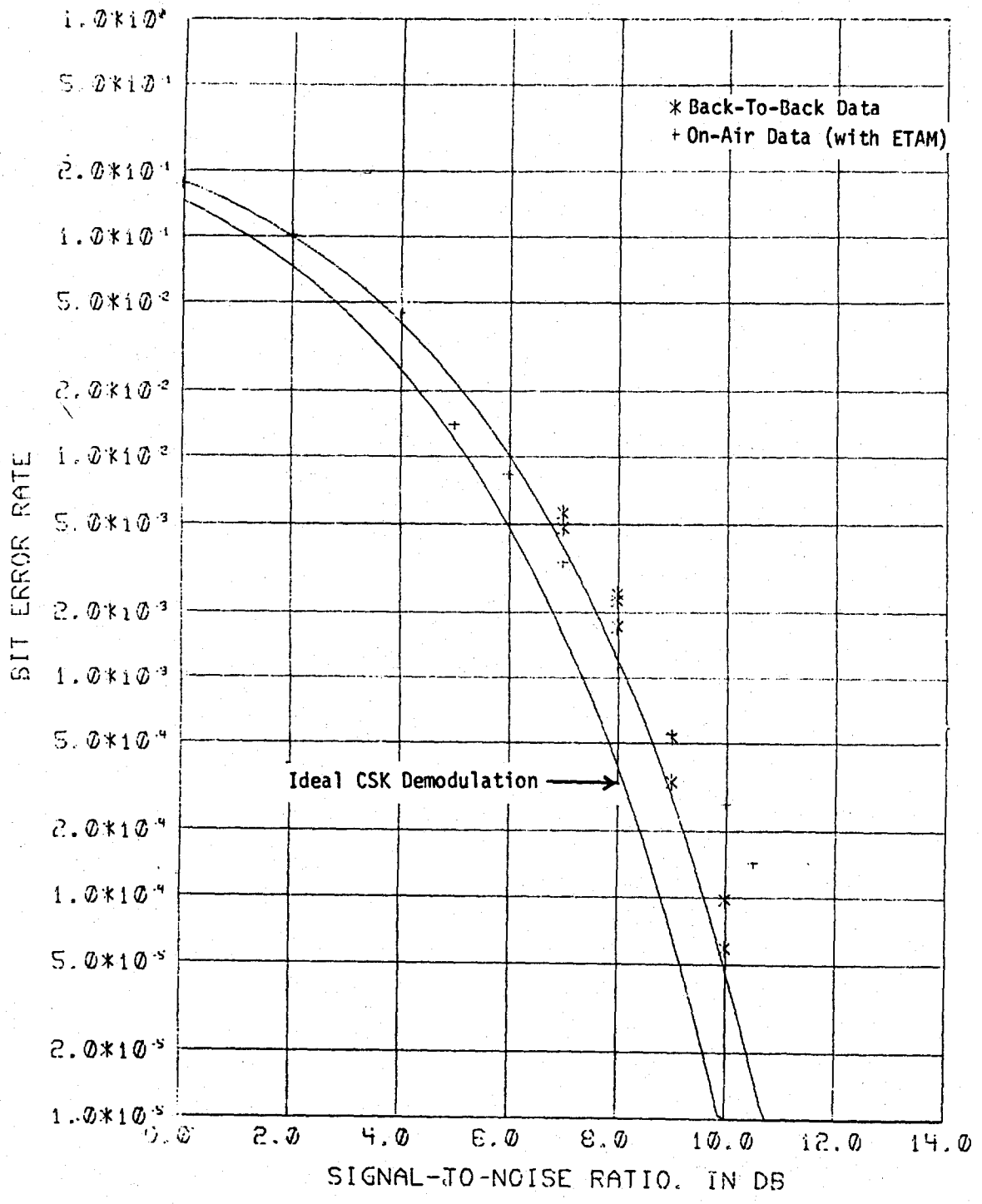

Figure 18. Compatible Shift Keying (CSK) Modem Performance

BIBLIOGRAPHY

1. Galejs,J.,"Electronic Broadbanding of High-Q Tuned Circuits or Antennas," *Archiv der Elektrischen Ubertragung,* Vol. 17, 1963, Part 8, pp. 375-380.

2. Hartley, H. F., "Electronic Broadbanding of VLF/LF Antennas for FSK Radio Communication," *IEEE Transactions on Communication Technology,* Vol. COM 19, No. 4, August 1971, pp. 555-561.

3. Hartley, H. F., and M. L. Jones, "Experimental Transmitting Antenna Modulator," Baltimore, Maryland, RADC TR-72-212 (Contract F30602-72-C-0051), August 1972, AD #904073L.

4. Ku, W. H., "Some Results in the Theory of Optimum Broad-Band Matching," *IEEE Transactions on Circuit Theory,* Vol. CT-17, No. 3, August 1970, pp. 420-423.

5. Vallese, L. M., "Long Distance VLF/LF Radio Communication Systems," *Proc. IEEE International Communications Conference,* Minneapolis, Minnesota, June 1967, p. 41.

6. Watt, A. D., *VLF Radio Engineering,* Pergamon Press, New York, 1967.

APPENDIX A

Compatible Shift Keying (CSK) Modem

The compatibie shift keying (CSK) system is a coherent frequency shift keying modem which uses a modulation index of 1/2.

A1. Signal Structure and Relationship of Detector Decision Error Rate and Bit Error Rate.

The basic demodulation process is identical with that of the Collins Minimum Shift Keyed (MSK) system. This process can be best explained by considering the mathematical expression for the CSK waveform. Here, the CSK signal is given by

$$s(t) = KS \cos\left(\omega_c + \ell \frac{\pi t}{2T}\right) \qquad \text{(A-1)}$$

where T is the duration of a binary element, $\ell = \pm 1$ according to the data state (thus producing the FSK modulation), $K = \pm 1$ so as to maintain phase continuity at frequency shifts, and S is the signal amplitude.

Rewriting, we have

$$s(t) = KS \cos \omega_c t \cos \ell \frac{\pi t}{2T}$$

$$- KS \sin \omega_c t \sin \ell \frac{\pi t}{2T} \qquad \text{(A-2)}$$

It is readily seen that the first term is independent of the value of ℓ. Moreover, at $t = \pm 2nT$, $n = 0, 1, 2$, the first term has an envelope maximum so that K must remain constant at these points to maintain waveform continuity.

On the other hand, the second term changes sign as ℓ changes sign so that when frequency shifts occur at $t = (1 \pm 2n)T$, $n = 0, 1, 2$, K must change sign to maintain waveform continuity. This effectively produces an RF phase reversal in the first term at an envelope zero.

Thus, the effect of frequency shift keying is to produce sequential phase reversals in the two quadrature terms of S(t). Here, MSK detectors can be used to demodulate the phase modulation of these two quadrature components of the signal. However, the information is not contained in the phase state *per se;* it is contained in the frequency state. This is readily handled, nevertheless, as the instantaneous frequency is directly defined by the phase difference of these two components. That is, expressing the first component as

$$C(t) = S \cos \frac{\pi t}{2T} \sin(\omega_c t + \phi_c) \qquad \text{(A-3)}$$

and the second component as

$$S(t) = S \sin \frac{\pi t}{2T} \cos(\omega_c t + \phi_s) \qquad \text{(A-4)}$$

where $\phi_c, \phi_s = \pm \frac{\pi}{2}$, the upper shift frequency exists when $\phi_c - \phi_s = 0$, and the lower shift frequency exists when $|\phi_c - \phi_s| = \Pi$.

Thus, the data is recovered from quadrature MSK detectors according to the difference (modulo 2Π) of their indicated phase state. This differential post-detection process obviously produces a sequential pair of binary output errors for each isolated MSK-detector phase-decision error.

This means that the output bit error rate (BER) is asymptotically twice the detector-decision-error rate as the decision error rate tends to zero. Conversely, in the case where the detector-decision-error rate is relatively high, time adjacent decision errors become more probable so that the output bit error rate approaches the decision error rate as the latter approaches its upper bound of .5 (binary error rate produced by random noise only, assuming the post-detection noise statistic is a zero-mean random variable). However, a closed form relationship between output BER and decision error rate is not apparent. Thus, numerical means have been employed to estimate this relationship.

Figure A1 shows the quantitative relationship between output BER as a function of detector-decision-error rate where differential post-detection processing is employed. (Here, it is apparent that the actual output BER rapidly approaches a value of twice the decision error rate as the decision error rate tends to zero.) This result will be combined with the decision error rate derivation of Section A2 to derive a theoretical error rate for the CSK demodulator in Section A3.

A2. MSK Detection Process

From Section A1, decision element signal components c(t) and S(t) are given by (A-3) and (A-4) respectively. Because of the similarity of these elements, it is sufficient to examine either to determine the overall probability of decision error. In this case, consider the detection element whose signal component remains constant over the interval (0, 2T). This is S(t), given by (A-4) as

$$S(t) = S \sin \frac{\pi t}{2T} \cos (\omega_c t + \phi_s)$$

where $$\phi_s = \pm \frac{\pi}{2}, \quad 0 \leq t \leq 2T$$

Assuming that $\Pr (\phi_s = \frac{\pi}{2}) = \Pr (\phi_s = -\frac{\pi}{2}) = \frac{1}{2}$

we may arbitrarily choose $\phi_s = \frac{\pi}{2}$ without loss of generality. Thus, the signal component becomes

$$S(t) = -S \sin \frac{\pi t}{2T} \sin \omega_c t \qquad \text{(A-5)}$$

Now, returning to a consideration of the general coherent (matched filter) detection process, in general a coherent receiver functions as depicted below.

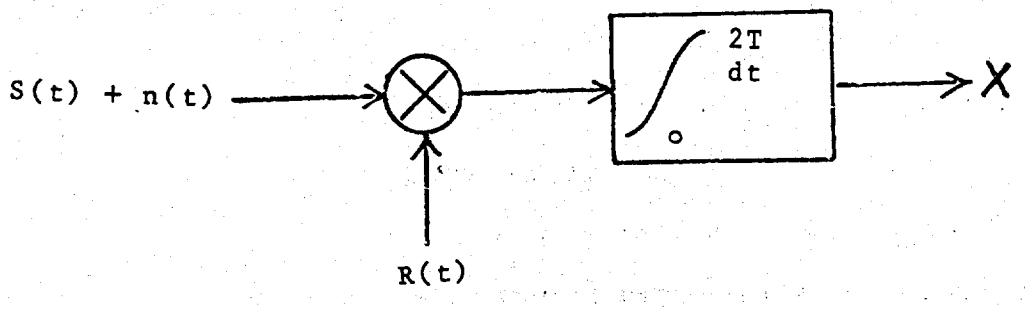

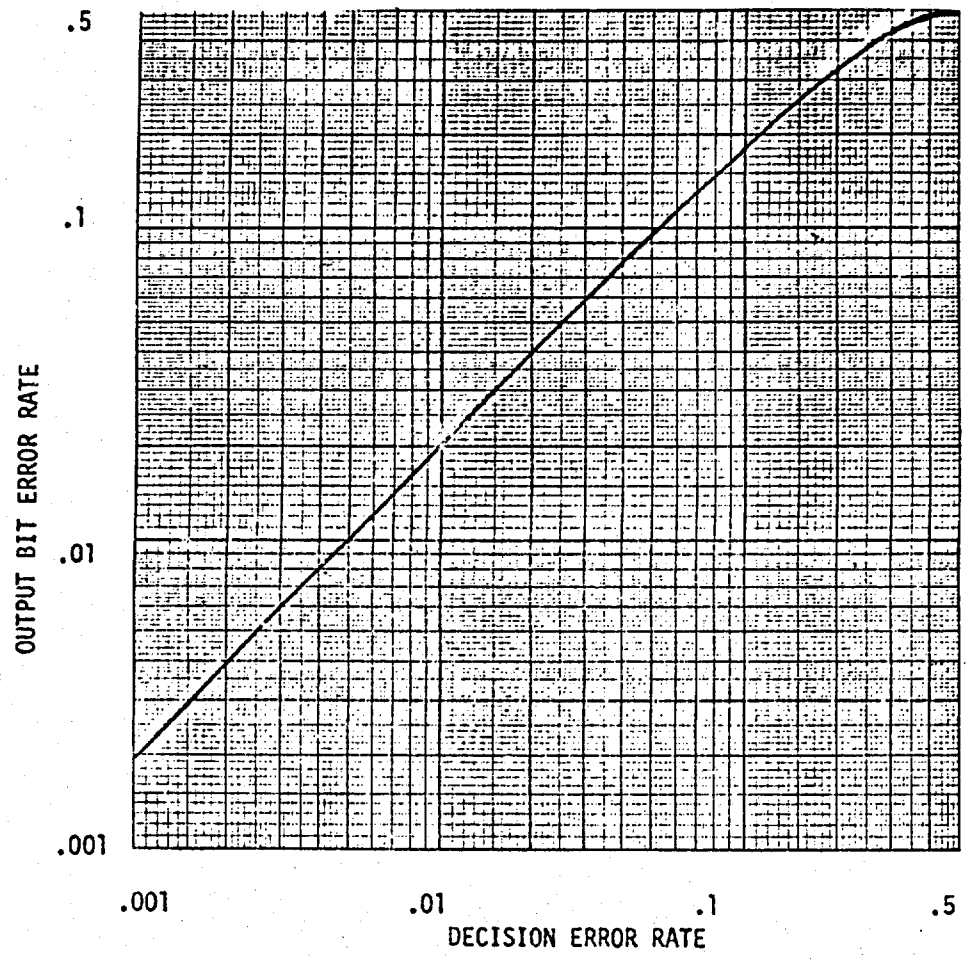

Figure A1. Output Bit Error Rate vs. Decision Error Rate (Differential Decoding)

Here, the signal, s(t), and additive, white, zero-mean, Gaussian noise process, n(t), are multiplied by the coherent receiver reference signal R(t), and integrated over the period of a decision element (2T). The detector decision is then based on the sign of the detector functional X. Here X is given by

$$X = \int_0^{2T} R(t)\,[S(t) + n(t)]\,dt \tag{A-6}$$

In this case, the coherent receiver reference signal, R(t), is given by

$$R(t) = S \sin \frac{\pi t}{2T} \sin \omega_c t \tag{A-7}$$

Expressing n(t) in a narrow band representation, we have

$$n(t) = n_c(t) \cos \omega_c t - n_s(t) \sin \omega_c t \tag{A-8}$$

where $n_c(t)$ and $n_s(t)$ are uncorrelated zero mean Gaussian processes.

Substituting (A-5), (A-7) and (A-8) into (A-6), we have

$$X = \int_0^{2T} S \sin \frac{\pi t}{2T} \sin \omega_c t \left[-S \sin \frac{\pi t}{2T} \sin \omega_c t + n_c(t) \cos \omega_c t - n_s(t) \sin \omega_c t\right] dt \tag{A-9}$$

Disregarding high frequency components in the integrand of (A-9), we have

$$X \approx \frac{1}{2}\int_0^{2T}\left[-S^2 \sin^2\frac{\pi t}{2T} - S n_s(t)\sin\frac{\pi t}{2T}\right] dt \tag{A-10}$$

$$= \frac{S}{2}\int_0^{2T}\left[-\frac{S}{2} + \frac{S}{2}\cos\frac{\pi t}{T} - n_s(t)\sin\frac{\pi t}{2T}\right] dt \tag{A-11}$$

Now, computing the mean, we find

$$\bar{X} = \frac{S}{2}\int_0^{2T}\left[-\frac{S}{2} + \frac{S}{2}\cos\frac{\pi t}{T} - E\left\{n_s(t)\right\}\sin\frac{\pi t}{2T}\right] dt$$

$$= \frac{S^2 T}{2} \tag{A-12}$$

We also find the variance of X, given by Var (X) $\triangleq \overline{X^2} - \bar{X}^2$, which from (A-10) and (A-12), becomes

$$\text{Var}(X) = E\left\{\frac{S^2}{4}\int_0^{2T} dt_1 \int_0^{2T} dt_2 \left[-S\left(\sin\frac{\pi t_1}{2T}\right)^2 - n_s(t_1)\left(\sin\frac{\pi t_1}{2T}\right)\right]\left[-S\left(\sin\frac{\pi t_2}{2T}\right)^2 - n_s(t_2)\left(\sin\frac{\pi t_1}{2T}\right)\right]\right\}$$

$$-\frac{S^4T^2}{4}$$

$$= \frac{S^2}{4}\int_0^{2T} dt_1 \int_0^{2T} dt_2 \left[S^2\left(\sin\frac{\pi t_1}{2T}\right)^2\left(\sin\frac{\pi t_2}{2T}\right)^2 + E\left\{n_s(t_1)\right\} S \sin\frac{\pi t_1}{2T}\left(\sin\frac{\pi t_2}{2T}\right)^2 + E\left\{n_s(t_2)\right\} S \sin\frac{\pi t_2}{2T}\left(\sin\frac{\pi t_1}{2T}\right)^2 + E\left\{n_s(t_1)\, n_s(t_2)\right\}\sin\frac{\pi t_1}{2T}\sin\frac{\pi t_2}{2T}\right]$$

$$- \frac{S^4T^2}{4} \tag{A-13}$$

Now recalling that $n_s(t)$ is a white noise process, we assume its power spectral density is $\frac{N_o}{2}$ watts/Hz. Using the Wiener Khintchine theorem, we find

$$E\left\{n_s(t_1)\, n_s(t_2)\right\} = \int_{-\infty}^{\infty}\frac{N_o}{2} e^{j2\pi f(t_1 - t_2)} df$$

$$= \frac{N_o}{2}\delta(t_1 - t_2), \qquad 0 \leq t_1, t_2 \leq 2T \tag{A-14}$$

where δ [ ] is the Dirac Delta function.

Substituting (A-14) into (A-13), we have

$$\text{Var}[X] = \frac{S^2 N_o}{8} \int_o^{2T} dt_1 \int_o^{2T} dt_2 \, \delta(t_1 - t_2) \, X \cdot \sin \frac{\pi t_1}{2T} \sin \frac{\pi t_2}{2T}$$

$$= \frac{S^2 N_o}{8} \int_o^{2T} \sin^2 \frac{\pi t_1}{2T} \, dt_1$$

$$= \frac{S^2 N_o T}{8} \qquad \text{(A-15)}$$

Now, since the input to the integrator is Gaussian, and the integration is a linear process, the functional X which results from the integration is also Gaussian. Thus, the probability density of the random variable X can be completely described by its mean, $\overline{X}$, and its variance. Using (A-12) and (A-15), we have the probability density of X given by

$$f_X(x) = \frac{1}{\sqrt{2\pi}\sqrt{\frac{S^2 N_o T}{8}}} \text{Exp}\left\{ - \frac{4\left(x + \frac{S^2 T}{2}\right)^2}{S^2 N_o T} \right\}$$

$$= \frac{2}{S\sqrt{\pi N_o T}} e^{- \frac{(2X + S^2 T)^2}{S^2 N_o T}} \qquad \text{(A-16)}$$

Since a decision error occurs when $X > 0$, the probability of a decision error is given by

$$P_e = \int_o^{\infty} f_X(X) \, dX$$

$$= \frac{2}{S\sqrt{\pi N_o T}} \int_o^{\infty} e^{- \frac{(2X + S^2 T)^2}{S^2 N_o T}} \, dX$$

$$= \frac{1}{\sqrt{\pi}} \int_{\frac{ST}{\sqrt{N_o T}}}^{\infty} e^{-u^2} \, du$$

$$\left(\text{by the substitution } U = \frac{2X + S^2 T}{S\sqrt{N_o T}} \right)$$

$$= \frac{1}{2}\left[1 - \text{Erf}\left(\sqrt{\frac{S^2/2}{N_o/2T}} \right) \right] \qquad \text{(A-17)}$$

Recall that if S is the amplitude of the sinusoidal signal, then $S^2/2$ is the signal power. Likewise, if each data element is T seconds, then the overall detection bandwidth is 1/T Hz and thus, $N_o/2T$ is the noise power referenced to the detection bandwidth. Hence, the argument of Erf [ ] in (A-17) is simply the square root of the signal-to-noise ratio referenced to the detection bandwidth. This result is identical to that obtained for coherent-biphase or quadriphase, phase shift keying (PSK) which is classically analyzed in the literature and determined to afford optimum detection efficiency. This is illustrated by Figure A2 wherein the probability of MSK decision error is presented as a function of signal-to-noise ratio referenced to the detection bandwidth.

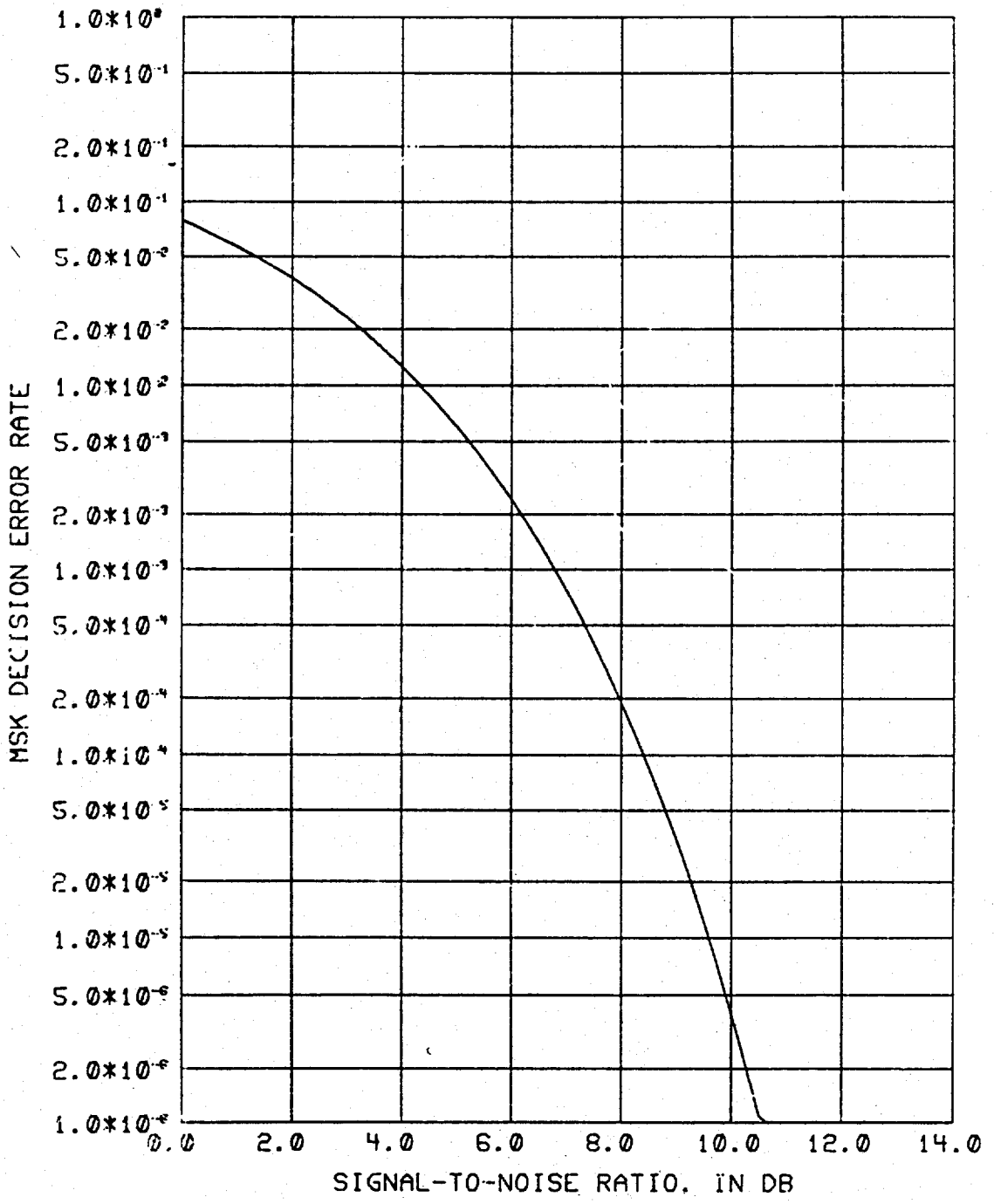

Figure A2. Decision Error Rate for MSK Detection

A3. CSK Output Bit Error Rate

In order to determine the output bit error rate of the CSK demodulator, it is necessary to consider the effect of the differential post-detection decoding. This is accomplished by integrating the numerically derived results of Figure A1, which show the relationship between input decision error rate and output differentially-derived bit error rate, and the theoretically derived results of Figure A2, the decision error rate. This is presented in Figure A3.

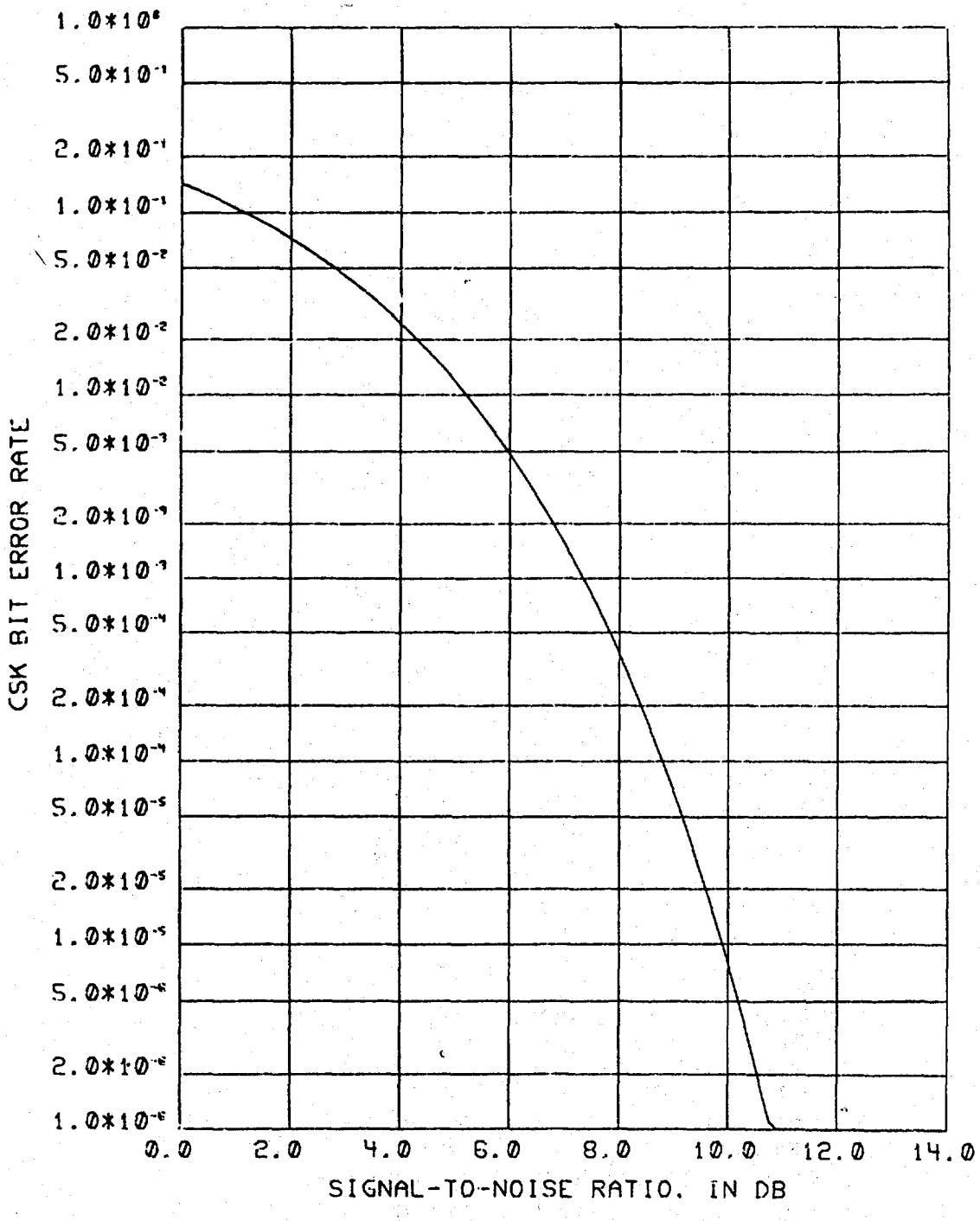

Figure A3. Output Bit Error Rate for CSK Demodulation

APPENDIX B
REACTANCE MODULATION OF VLF ANTENNAS

1. Passive Equivalent of VLF Antenna Circuit.

In Figure B1, a passive network is shown which closely approximates the electrical characteristics of an electrically small antenna. The term "electrically small" is appropriate when the operating frequency is much less than the natural dipole resonance frequency of the antenna system, or, in other words, the length of the antenna is much less than 1/4 the free-space wavelength of the signal to be transmitted. Under this condition, the antenna structure is effectively a series capacitance and resistance. Because of the electrical shortness of the antenna, both the capacitance, C_a, and the radiation resistance, R_r, are necessarily small. The loss resistance, R_i, produced by ohmic losses in the antenna and ground system is customarily minimized in design and construction so as to maximize efficiency; the antenna efficiency is given by

$$\eta = \frac{R_r}{R_r + R_L} \qquad \text{(B-1)}$$

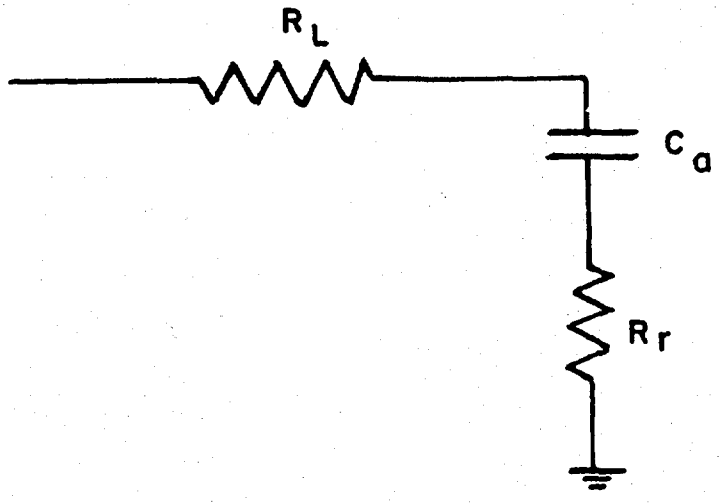

Figure B1. Passive Equivalent of Electrically Small Antenna

However, the low value of capacitance of the antenna structure causes such a short monopole to be a highly reactive electrical load for a power transmitter. This is compensated for by the inclusion of a series inductor or helix of proper inductance to produce series resonance, and hence, a resistive transmitter load, at the desired frequency. This typical low frequency equivalent antenna circuit is shown in Figure B2.

Just as the inherent antenna and ground losses must be minimized for system efficiency, so must the ohmic losses in the tuning inductance; in Figure B2, the resistance of the coil is combined with the other antenna system loss resistances in the term R_L, and R_g is the source resistance of the transmitter amplifier represented in Thevenin equivalent form.

The subsequent discussions will specifically address the operation of this passive RLC circuit as a close approximation of the actual VLF antenna system. Here, the equivalent circuit will be analyzed for a constant amplitude FSK driving signal and stepwise modulation of the circuit inductance so as to tune the circuit to resonance in synchronism with the FSK modulation.

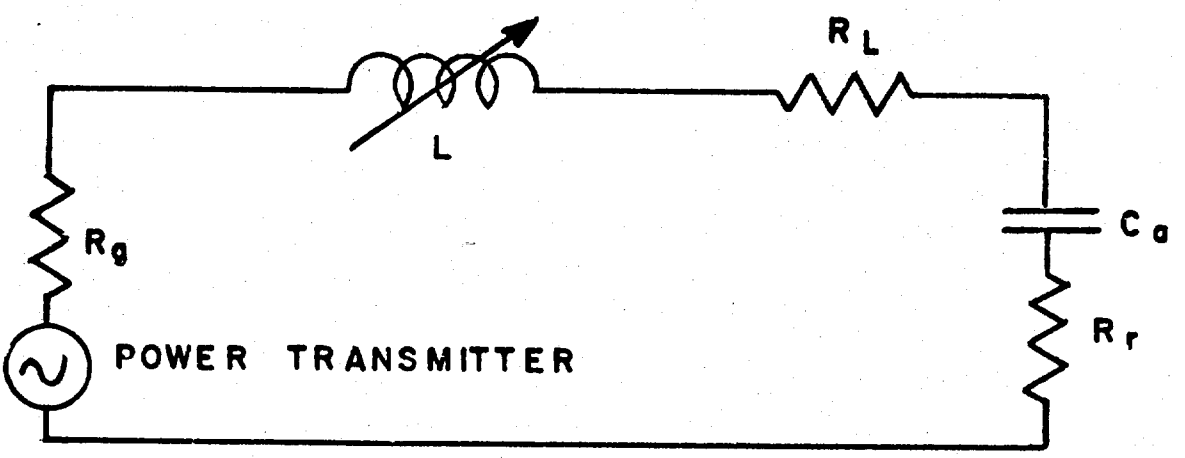

Figure B2. Passive Equivalent Circuit of a VLF/LF Antenna System

2. Circuit Analysis

In the circuit of Figure B2, the electrostatic charge on the capacitor, Q(t), is given by the following differential equation:

$$L\frac{d^2q}{dt^2} + R\frac{dq}{dt} + \frac{1}{C_a}q = V(t), \quad t<0$$

or

$$\frac{d^2q}{dt^2} + \frac{R}{L}\frac{dq}{dt} + \frac{1}{LC_a}q = \frac{1}{L}V(t), \quad t<0 \qquad \text{(B-2)}$$

where $R = R_g + R_L + R_r$ and V(t) is the driving voltage output of the transmitter amplifier.

The above equation (B-2) may also be written as

$$\frac{d^2q}{dt^2} + 2\alpha\frac{dq}{dt} + \omega_o^2 q = \frac{1}{L}V(t), \quad t<0$$

where $\alpha = \frac{R}{2L}$ and $\omega_o = \sqrt{\frac{1}{LC_a}}$ (B-3)

If the driving voltage has been

$$V(t) = A\sin\omega_o t, \quad (t<0) \qquad \text{(B-4)}$$

such that steady state conditions exist at t = 0, then the current, i(t), for $t \leq 0$ is given by

$$i(t) \approx \frac{V(t)}{R} = \frac{A}{R}\sin\omega_o t, \quad t \leq o \qquad \text{(B-5)}$$

provided $\alpha^2 << \omega^2$, which is the usual condition in the high-Q antenna network.

Recognizing that $i(t) = \frac{dq}{dt}$ and thus substituting (B-5) and (B-4) in (B-3), we obtain

$$q(t) = -\frac{A}{R\omega_o} \cos \omega_o t, \quad t \leqslant 0 \tag{B-6}$$

In addition

$$q(0) = -\frac{A}{R\omega_o}$$

$$q'(0) = 0 \tag{B-7}$$

Now let us assume that at the next zero crossing of the driving voltage (at t = 0), the inductance is changed by ΔL. This yields a series resonance frequency of

$$\omega_1 = \frac{1}{\sqrt{(L + \Delta L) C_a}}, \quad t \geqslant 0 \tag{B-8}$$

Further, assuming the driving voltage is simultaneously changed in frequency to ω_1, we have

$$V(t) = A \sin \omega_1 t, \quad t \geqslant 0 \tag{B-9}$$

Here, the differential equation of the circuit now becomes

$$\frac{d^2q}{dt^2} + 2a_1 \frac{dq}{dt} + \omega_1{}^2 q = \frac{A}{(L + \Delta L)} \sin \omega_1 t$$

where $a_1 = \frac{R}{2(L + \Delta L)}, \quad t \geqslant 0$ (B-10)

Now, taking Laplace transforms of both sides of this equation, we have

$$S^2Q(S) - Sq(0) - q'(0) + 2a_1SQ(S)$$
$$-2a_1q(0) + \omega_1{}^2 Q(S) =$$
$$\frac{A}{(L + \Delta L)} \cdot \frac{\omega_1}{S^2 + \omega_1{}^2} \tag{B-11}$$

From (B-6) we found that

$$q'(0) = 0, \quad q(0) = -\frac{A}{R\omega_o} \tag{B-7}$$

and, substituting (B-7) in (B-11), we have

$$Q(S) = -\frac{A}{R\omega_o} \frac{S^3 + 2a_1 S^2 + \omega_1{}^2 S + 2a_1 \omega_1 (\omega_1 - \omega_o)}{(S^2 + \omega_1{}^2)(S^2 + 2a_1 S + \omega_1{}^2)} \tag{B-12}$$

This can be partitioned to yield

$$Q(S) = -\frac{A}{R\omega_o}\left[\frac{\omega_o}{\omega_1}\frac{S}{S^2+\omega_1^2} + \frac{\omega_1-\omega_o}{\omega_1}\frac{S+2a_1}{S^2+2a_1S+\omega_1^2}\right] \qquad \text{(B-13)}$$

Inversion of (B-13) yields

$$q(t) = -\frac{A}{R\omega_o\,\omega_1}\left[\omega_o\cos\omega_1 t + (\omega_1-\omega_o)\,e^{-a_1 t}\cos\omega_N t + \frac{a_1}{\omega_N}(\omega_1-\omega_o)\,e^{-a_1 t}\sin\omega_N t\right]$$

where $\omega_N = \sqrt{\omega_1^2 - a_1^2}$ (B-14)

Since $\omega_1^2 >> a_1^2$, $\omega_N \approx \omega_1$. Using this approximation and differentiating (B-14) we obtain i(t):

$$i(t) = -\frac{A}{R\omega_o\,\omega_1}\left[-\omega_o\,\omega_1\sin\omega_1 t - \left(\omega_1+\frac{a_1^2}{\omega_1}\right)(\omega_1-\omega_o)\,e^{-a_1 t}\sin\omega_1 t\right]$$

$$= \frac{A}{R}\left[1+\frac{\omega_1-\omega_o}{\omega_o}\left(1+\frac{a_1^2}{\omega_1^2}\right)e^{-a_1 t}\right]\sin\omega_1 t$$

$$i(t) \approx \frac{A}{R}\left[1+\frac{\omega_1-\omega_o}{\omega_o}\,e^{-a_1 t}\right]\sin\omega_1 t \qquad \text{(B-15)}$$

This result clearly shows the steady state and transient terms in the current amplitude or waveform envelope. Since the above result was not dependent on the sign of ΔL, it must hold for both positive and negative frequency shifts. In the case of a positive frequency shift $\omega_1 > \omega_o$ so that the current amplitude (waveform envelope) increases by $(\omega_1 - \omega_o)/\omega_o$ relative to the steady state value immediately upon the frequency, and corresponding inductance, shift. On the other hand, a frequency downshift gives $\omega_1 < \omega_o$ so that the current amplitude decreases by $(\omega_1 - \omega_o)/\omega_o$ relative to the steady state value upon the frequency and inductance shift. It should be noted that the maximum value of the transient term (in either case) is a small fraction of the steady state current amplitude since $|\omega_1 - \omega_o| << \omega_o, \omega_1$ and this implies $|(\omega_1 - \omega_o)/\omega_o| << 1$. Further examination of (B-15) shows that the amplitude transient term decays toward zero exponentially with time, with a time constant, a_1, given by

$$a_1 = \frac{R}{2(L+\Delta L)} \qquad \text{(B-16)}$$

where R is the total circuit resistance and $(L + \Delta L)$ is the total circuit inductance after the frequency and inductance shift.

Consequently, the circuit current tends to its steady state value as the amplitude transient term tends to zero, exponentially with time.

Static Bandwidth Considerations

Finally, it is appropriate to examine the relationship between the antenna circuit static bandwidth and the previously obtained current amplitude transient time constant a_1. Recalling the differential equation of the circuit as tuned for frequency ω_1 (B-10) and assuming a unit impulse input ($V(t) = \delta(t)$), the Laplace transform is given by

$$S^2 Q(S) - Sq(0) - q'(0) + 2a_1 SQ(S) - 2a_1 q(0) + \omega_1^2 Q(S) = \frac{1}{L + \Delta L} \qquad \text{(B-17)}$$

Further, assuming $q(0) = q'(0) = 0$, this yields

$$Q(S) = \frac{1}{(L + \Delta L)(S^2 + 2a_1 S + \omega_1^2)} \qquad \text{(B-18)}$$

Finally, recognizing that the transform of the current response I(S), is given by

$$I(S) = \mathcal{L}(q'(t)) = SQ(S) \qquad \text{(B-19)}$$

we obtain

$$I(S) = \frac{S}{(L + \Delta L)(S^2 + 2a_1 S + \omega_1^2)} \qquad \text{(B-20)}$$

which is the Laplace transform of the network current impulse response.

Now, replacing S by $j\omega$ in (B-20), we obtain the Fourier transform. Multiplication of $I(j\omega)$ by its complex conjugate $I^*(j\omega)$ yields $I(j\omega')$.

$$|I(j\omega)|^2 = \frac{\omega^2}{(L + \Delta L)^2 [(\omega_1 - \omega)^2 + 4a_1^2 \omega^2]} \qquad \text{(B-21)}$$

Here, the maximum power is obtained at $\omega = \pm \omega_1$; thus, the 3 db, or half-power, bandwidth is given by the difference of the positive roots, X_1, X_2 of

$$|I(jX)|^2 = \frac{1}{2} |I(j\omega_1)|^2 \qquad \text{(B-22)}$$

This becomes

$$\frac{X^2}{(\omega_1^2 - X^2)^2 + 4a_1^2 X^2} = \frac{1}{8a_1^2}$$

$$\text{or } X^4 - 2(\omega_1^2 + 2a_1^2) X^2 + \omega_1^4 = 0 \qquad \text{(B-23)}$$

Hence,

$$X^2 = \omega_1^2 \pm 2a_1\omega_1\sqrt{1 + \frac{a_1^2}{\omega_1^2}} + 2a_1^2$$

$$\approx \omega_1^2 \pm 2a_1\omega_1 + 2a_1^2$$

since $\omega_1^2 >> a_1^2$ (B-24)

The larger positive root, X_1, is given by:

$$X_1 = \omega_1\sqrt{1 + \frac{2a_1}{\omega_1} + \frac{2a_1^2}{\omega_1^2}}$$

$$\approx \omega_1\left(1 + \frac{a_1}{\omega_1}\right) \quad \text{(B-25)}$$

and the smaller, X_2, by

$$X_2 \approx \omega_1\left(1 - \frac{a_1}{\omega_1}\right) \quad \text{(B-26)}$$

Finally, the 3 db bandwidth, B_3 is given by

$$B_3 = X_1 - X_2 = 2a_1 \text{ Radians/sec}$$

$$= \frac{a_1}{\pi} \text{ Hz} \quad \text{(B-27)}$$

This result shows that the time constant governing the convergence of the current waveform envelope to its steady state value is π times the 3 db static bandwidth in Hz. Thus, the network static bandwidth is related to the transient component decay rate, but not the maximum size of the transient; the size of the transient, as shown by (B-15), is effectively a function of the shift frequencies involved (provided that these frequencies are much greater than zero as in a VLF radio system).

UNCLASSIFIED

SECURITY CLASSIFICATION OF THIS PAGE *(When Data Entered)*

REPORT DOCUMENTATION PAGE		READ INSTRUCTIONS BEFORE COMPLETING FORM
1. REPORT NUMBER RADC-TR-73-287	2. GOVT ACCESSION NO.	3. RECIPIENT'S CATALOG NUMBER
4. TITLE *(and Subtitle)* WIDEBAND COHERENT COMMUNICATION AT VLF WITH THE EXPERIMENTAL TRANSMITTING ANTENNA MODULATOR (ETAM)		5. TYPE OF REPORT & PERIOD COVERED In-house Final Report 6. PERFORMING ORG. REPORT NUMBER N/A
7. AUTHOR(s) John T. Gamble		8. CONTRACT OR GRANT NUMBER(s) N/A
9. PERFORMING ORGANIZATION NAME AND ADDRESS RADC/DCCL Griffiss AFB NY 13441		10. PROGRAM ELEMENT, PROJECT, TASK AREA & WORK UNIT NUMBERS 01710108
11. CONTROLLING OFFICE NAME AND ADDRESS Rome Air Development Center (DCCL) Griffiss Air Force Base, New York 13441		12. REPORT DATE December 1973 13. NUMBER OF PAGES 44
14. MONITORING AGENCY NAME & ADDRESS *(if different from Controlling Office)* Same		15. SECURITY CLASS. *(of this report)* Unclassified 15a. DECLASSIFICATION/DOWNGRADING SCHEDULE N/A

16. DISTRIBUTION STATEMENT *(of this Report)*

Distribution limited to U. S. Gov't agencies only; test and evaluation; December 1973. Other requests for this document must be referred to RADC (DCCL), GAFB, NY 13441.

17. DISTRIBUTION STATEMENT *(of the abstract entered in Block 20, if different from Report)*

Same

18. SUPPLEMENTARY NOTES

This effort was funded by the Laboratory Directors' Fund, Project 01710108.

19. KEY WORDS *(Continue on reverse side if necessary and identify by block number)*

Antenna Systems
VLF Radio Transmission
Modulation
Demodulation

20. ABSTRACT *(Continue on reverse side if necessary and identify by block number)*

A 1-kilowatt Experimental Transmitting Antenna Modulator (ETAM) was tested on-air at RADC. This on-air performance evaluation at 29.5 kHz employed a VLF transmitting station at Camden, New York and a receiving station at RADC, Griffiss AFB, New York. Using the ETAM, an 800 baud coherent FSK (Modulation Index of 1/2) signal was efficiently transmitted over the 160 Hz 3 dB static bandwidth transmitter/antenna system; concurrently, the signal was received and coherently demodulated with negligible evidence of intersymbol or other

DD FORM 1 JAN 73 1473 EDITION OF 1 NOV 65 IS OBSOLETE

UNCLASSIFIED

SECURITY CLASSIFICATION OF THIS PAGE *(When Data Entered)*

Block 20. ABSTRACT (Cont'd)

system degradation. On the other hand, when the ETAM was removed from the transmission system, it was necessary to derate the transmitter output by 10 db to preclude destruction of the transmitter output transformer caused by the high-Q mismatched output load; under this operating condition, it was impossible to obtain bit error rates less than 6% because of the ambient atmospheric noise and intersymbol distortion. This report describes the equipment configurations at the transmitter and receiver, the test procedures, and the quantitative results.

SAC--Griffiss AFB NY